Coordination Chemistry Reviews 254 (2010) 677–695

Contents lists available at ScienceDirect

Coordination Chemistry Reviews

journal homepage: www.elsevier.com/locate/ccr

Review

Halogen bonding in metal–organic–supramolecular networks

Roberta Bertani[a,*], Paolo Sgarbossa[a], Alfonso Venzo[b], Francesco Lelj[c], Mario Amati[c], Giuseppe Resnati[d,e], Tullio Pilati[e], Pierangelo Metrangolo[d], Giancarlo Terraneo[d]

[a] Department of Chemical Processes of Engineering, University of Padova, via F. Marzolo, 9, I-35131 Padova, Italy
[b] Istituto di Scienze e Tecnologie Molecolari del CNR (CNR-ISTM), via F. Marzolo, 9, I-35131 Padova, Italy
[c] Department of Chemistry, University of Basilicata, via N. Sauro 85, I-85100 Potenza, Italy
[d] NFMLab and CNSC-IIT@POLIMI: Department of Chemistry, Materials and Chemical Engineering "Giulio Natta", Politecnico di Milano; via Mancinelli 7; I-20131 Milano, Italy
[e] Istituto di Scienze e Tecnologie Molecolari del CNR (CNR-ISTM), Via Venezian 21, I-20133 Milano, Italy

Contents

ARTICLE INFO

Article history:
Received 27 July 2009
Accepted 27 September 2009
Available online 2 October 2009

Dedicated to Prof. Fausto Calderazzo, thanking for his great contribution to inorganic and metallorganic chemistry.

Keywords:
Halogen bonding
Supramolecular coordination chemistry
Metal halides
Metal cyanides
Halopyridines
Tetrathiafulvalenes
Hybrid perovskites
Alkynyl systems
Metal hydrides
Computational modelling

ABSTRACT

Halogen bonding (XB) has been recently exploited as a significant tool for engineering crystals involving coordination and organometallic compounds as tectons. This review, in particular, focuses on extended networks based on XB between electron donor groups bound to metals and halo-pyridine and halo-tetrathiafulvalene moieties as electron acceptors. The influence of XB over the structures and the interactions between the organic frameworks and the metal centers is highlighted. The chemistry of some mononuclear systems forming XB is described in terms of tools for controlling supramolecular arrangement and chemical behaviour. Various computational studies on the energy of XB at different levels of sophistication, their advantages and limits concerning the evaluation of the interaction energy and modelling of its origin are critically surveyed. Modelling of a new example of interaction between Cp_2MH_2 (M = Mo, W) and CF_3I is reported together with the description of the electron density of the complex analyzed in terms of the Quantum Theory of Atoms in Molecules (QTAIM) model.

* Corresponding author.
E-mail address: roberta.bertani@unipd.it (R. Bertani).

0010-8545/$ – see front matter © 2009 Elsevier B.V. All rights reserved.
doi:10.1016/j.ccr.2009.09.035

1. Introduction

Halogen bonding (XB) is any D···X–Y interaction wherein X is an electrophilic halogen atom (Lewis acid, halogen bonding donor), D is an electron density donor (Lewis base, halogen bonding acceptor) and Y is C, N, halogen, etc. [1–3]. The effectiveness of XB in driving the formation of a multitude of supramolecular architectures having different and useful properties [4–8] has already been proven. A wide variety of halogen bonding acceptors has been used, either neutral (most frequently pyridine, amine, carbonyl and ether moieties) or anionic [9–14]. Interestingly, simple ligands bound to transition metals or main group metals/metalloids may also serve as halogen bond acceptors, thus allowing for the design and synthesis of metal containing halogen bonded supramolecular architectures.

The use in supramolecular chemistry of modules containing metal centers [15] is of particular interest because metal ions (in charged or neutral coordination compounds) provide redox, magnetic, optical, and reactive properties that are not usually available in carbon based networks. Transition metals and lanthanoid ions are the more frequently employed. Transition metals, in fact, can be incorporated into networks as building blocks to direct a certain framework topology or can be used to introduce a particular electronic functionality [16,17]. Some of the specific advantages of introducing metals in supramolecular architectures are [18–24]:

(a) Metals provide a set of well defined coordination geometries, with ligand exchange kinetics that can allow for the reversible assembly–disassembly of supramolecular architectures, thanks to external stimuli and changes in the environment, with a switching of binding interactions by changing the redox state of the metal ion [25]. Strength and lability of the coordination bond allow for the ready and reversible synthesis of ordered materials so that errors in the self-assembly process can be corrected during the growth of periodic 1D, 2D, and 3D structures with crystallographic order.
(b) Metal–ligand bond distances are typically longer than those involving purely organic moieties leading to a large increase in the size of the channels and cavities that can be created within the structures. Interesting examples are represented by polyhedra, boxes and cages, whose properties are tuned in terms of dimensions, shape, and host guest chemistry [26,27].
(c) Metal complexes can be chiral not only in the case of a tetrahedral coordination but also in bis-bidentate $[M(A\text{-}A)_2]$, *cis*-bis-bidentate octahedral $[M(A\text{-}A)_2X_2]$, bis-tridentate octahedral $[M(A\text{-}A\text{-}A)_2]$, and tris-tridentate $[M(A\text{-}A\text{-}A)_3]$ complexes [28]. Chirality may also be present in the ligand. For these reasons polynuclear systems can contain a very large number of chiral stereocenters thus inducing the formation of chiral networks that can be used for asymmetric catalytic processes. Metal centers can also induce lack of symmetry into the network which is important in the pursuit of materials with second-order nonlinear optical (NLO), piezoelectric or ferroelectric behaviours [29].
(d) The occurrence of semioccupied d and f orbitals gives rise to strong absorption, high quantum yields, suitable excited state lifetimes, luminescence [30] and tunable redox states. These properties can be exploited to achieve optical non-linearity and photomediated charge separation for photovoltaic devices.
(e) The splitting of the d orbitals as a function of the magnitude of the ligand field strength can induce spin cross-over phenomena accompanied by a drastic change of physical properties [31]. Organometallic networks having M–C bonds with cyanide, or carbonyl, ligands, metallophilic and π interactions with electron rich aromatic systems (where short distances between adjacent metal ions are present) allow for a significant degree of communication thereby assisting in the construction of magnetically ordered solids [32].
(f) Many metal tectons are charged and the counter ions are not innocent bystanders [33]. They may eventually direct the structural topology of the metal containing networks by acting as templates [34]. The properties of the counter ions that may direct the structure include size, shape, ability to form hydrogen bonds (HB) and other weak interactions (such as π–π) and to induce charge polarization.

The role of XB in metal-containing crystal structures has been recently reviewed [35] and the focus was on the diversity of metal–ligand moieties that exhibit propensity to form XB. Analogies and differences with respect to HB have also been discussed [36]. The emphasis of this review on XB based coordination and metal–organic supramolecular networks will be on the nature and structures of the tectons and the relationship between the architecture of the self-assembled systems and their functional properties. Both theoretical aspects of XB and applied chemistry of halogen bonded systems will be discussed. A particular attention will be given to halogen bonded architectures showing interesting conductive and magnetic properties. The metal complexes assembled *via* XB and the resulting supramolecular synthons will be ordered according to Chart 1.

2. Halogen bonding: a theoretical and computational approach

2.1. Computational and interpretation tools

As all the low intensity "non-covalent" interactions in the sense of Lewis, XB represents a challenging target from a computational point of view. Different approaches have been followed for its theoretical study.

Different approaches can be followed for the purpose of a study. In the past *ab initio* Self Consistent Field (SCF) with orbitals expressed as Linear Combination of Atomic Orbitals (LCAO) computations where mainly of Hartree-Fock (HF) type. Nowadays the availability of computational codes that offer the possibility to take into account the electron correlation contribution, in implicit, perturbative or explicit way, where its difference to the relative energies of the adducts compared to the interacting fragments can give relevant contribution to the interaction energy, are now more frequently used.

These methods range from Density Functional Theory (DFT) recently reviewed on this journal [37], and Time Dependent DFT (TD-DFT) [38,39] to post-HF calculation using Many Body Perturbation Theory [40] of the Moller–Plesset (MP) kind. The MP2 (up to second order) offers the possibility to evaluate at a contained computational cost both energies, gradients and second derivatives as well. Furthermore refined correlation methods are Coupled Cluster [41] including Single and Double excitation (CCSD) but their computational effort become rapidly very elevated as soon as the number of basis set functions (large number of atoms and/or very accurate basis set) increases.

As far the interpretation of the different contribution perturbative expansion of the interaction energies [42] and different decomposition approaches are available [43–46]. Some interpretation tools are related to the computations of the molecular electrostatic potential [47] and the Electron Localization Function [48–50] (ELF) analysis and the electron density according to the Atom in Molecules (AIM) model of Bader [51] as well. Only the second to our knowledge has been used in the characterization of XB.

XB acceptor	XB donor		Interaction
Metal-X	X'-C(Y)	X = halogen;	M-X···X'-C(Y)
Metal-L	X'-C(Y)	L = CN, SCN;	M-L···X'-C(Y)
Metal-O	X'-C(Y)		M-L···X'-C(Y)
Metal-spacer-L'	X'-C(Y)	L' = pyridine;	M-spacer-L'···X'-C(Y)

In all of these cases X' = electrophilic halogen atom, and C(Y) is most often a pyridine or a tetrathiafulvalene moiety, or a fluorocarbon residue.

Chart 1. Synopsis of the different halogen bonding (XB) patterns in metal–organic–supramolecular networks.

Here we will not discuss the interactions regarding halogen molecules or interhalogen molecules with electron donors in the gas phase because a very exhaustive review has recently been published [52].

In 2000 Valerio et al. reported a detailed computational [53] study on XB by examining the case of the complexes of ammonia with CY_3X (Y = H, F; X = Cl, Br, I) and $CH_{(3-m)}F_mI$ (m = 0, 1, 2, 3), comparing both MP2 and DFT using Becke's exchange functional [54] and the Perdew's [55] correlation one. The basis set was of double zeta quality for the DFT calculations on all atoms whereas in the case of MP2 calculations a pseudopotential one was used for heavy atoms. The basis set superimposition error (BSSE) correction was larger for MP2 (∼26%) than DFT calculations (∼10%). The agreement between the MP2 and DFT, as far as the interaction energy is concerned, was within 0.6 kcal/mol (2.51 kJ/mol) for $CH_3I\cdots NH_3$ and $CF_3I\cdots NH_3$. The energy of the interaction was in the range between 2.3 and 6.4 kcal/mol (9.62 and 26.78 kJ/mol) for CF_3Cl and CF_3I, respectively. Furthermore, trifluorine substitution was more effective in increasing the interaction energy for CF_3Br than for the series of compounds $CH_{(n-m)}F_mI$ (m = 0, 1, 2). In all cases the interaction distance I···N decreased on increasing the number of fluorine atoms whereas the C–I distance increased with respect to the free molecule. The QTAIM approach was used to evaluate the net charge transfer from ammonia to the halogen, upon complex formation. As it could be expected, the degree of charge transfer increased on increasing the number of fluorine atoms. Similar results have been recently obtained [56] using hybrid [57] exchange correlation functional confirming the main picture previously reported.

A wider set of electron donor molecules $(CH_3)_nY$ (Y = N, P, n = 3; Y = S, n = 2) and $(CH_3)_nYO$ (Y = N, P, n = 3; Y = S, n = 2) interacting with CF_3I have been investigated [58] more recently in order to gain insight into the effect of the basis set, Effective Core Potentials (ECP), and the origin and nature of XB. To the best of our knowledge, this is the only study taking into account the contribution of the relativistic behaviour of the inner electrons even if at a scalar level [59]. The importance of relativistic effects at both geometry and energy bonding level has been highlighted by the fact that only if the relativistic geometry and energy are used, the trend of interaction energy reported in the literature N < P can be theoretically reproduced. The evaluation [60] of the C_6 van der Waals coefficient for $CF_3I\cdots N(CH_3)_3$ and $CF_3I\cdots P(CH_3)_3$ adducts according to the TD-DFT involving the asymptotically corrected Van Leeuwen–Baerends potential (LB94) [61] suggested that at least in the reported systems the estimated values of −2.02 (−4.45) and −1.30 (−5.43) kcal/mol (kJ/mol), respectively, for their dispersion energy, represent only a small contribution to the total bonding energy (−5.64 (−23.60) and −5.76 (−20.10) kcal/mol (kJ/mol), respectively). BSSE correction has been taken into account and energy decomposition analysis has been performed.

The set of studied donors offered the opportunity to evaluate the role of the substituent groups $(CH_3)_3P$ and $(CH_3)_2S$ on the ability of the electron donor atom, the oxygen, to be engaged in O···I interaction. The results indicated that the relative role of the electronic interaction between the residues $(CH_3)_nY$ (Y = N, P, n = 3; Y = S, n = 2) and O is responsible of the order of donor ability found in the case of compounds $(CH_3)_nYO$, Y = N > P > S. This suggested that the substituents on the donor atom has an active role in determining the mechanism of the interaction as it could be the case of halogen atoms bound to a transition metal. In this respect, even though some computations on some model systems involved in XB and containing metal atoms have been reported [62], they lack completely this kind of analysis taking into account only the molecular electrostatic potential.

Bianchi et al. [63] reported the QTAIM analysis of the electron density obtained by low temperature X-ray diffraction studies of the complex between (E)-1,2-bis(4-pyridyl)ethylene and 1,4-diiodotetrafluorobenzene. They found a tight analogy in the electronic properties between the I···N halogen bonding and a medium to strong HB, according to the properties Bond Critical Points (BCP). Forni [64] reported similar results in the case of the complexes of 1,4-dibromotetrafluorobenzene with dipyridyl derivatives. In both cases the QTAIM analysis of the experimental electron density was in agreement with high quality DFT calculations indicating the correctness of the description of this interaction.

A new type of XB, the so called blueshifting XB, has been investigated [65] in analogy to the blushifting HB. This latter is characterized by a contraction of the X–H bond and a blueshifting of the respective X–H stretching frequency, which is opposite to the conventional HB. According to calculations (MP2(full)/6-311++G(d,p) level) on the intermolecular interactions involving a series of representative blueshifting halogen-bonded complexes, the authors found that eleven halogen-bonded complexes exhibited blueshifting XB characters. In particular C–Cl, C–Br, Si–Cl, or N–Cl showed a decrease by 0.0053–0.0245 Å of the bond length upon interaction with a certain donor (NH_3, H_2O, Br^-) and the corresponding C–Cl, C–Br, Si–Cl, or N–Cl stretching frequencies were 3.2–20.6 cm^{-1} higher in the dimers than in the respective free monomers. By application of the QTAIM formalism to the blueshifting XB, the analysis pointed out the different physical nature of the blueshifting XB with respect to HB, on the basis of the electron density. A decreased density, in many cases, is found in the region between the C(Si, N) and Cl(Br) atoms. Though the blueshifting XB and HB are different in their physical nature, the negative permanent dipole moment of the donor molecule is responsible of the effect in both cases. The phenomenological behaviour of redshifting XB can be shown even in presence of the capability of forming a blueshifting XB or HB if the electric field from the acceptor is "strong" [66] enough at the equilibrium intermolecular distance.

A study [67] on the interaction between aromatic bromoderivatives with negative ions or neutral Lewis bases has been performed at the MP2 level with a large basis set followed by QTAIM analysis. The interaction strength decreases in the order $OH^- > F^- > HCO_2^- > Cl^- > Br^-$, and $H_2CS > H_2CO > NH_3 > H_2S > H_2O$. The authors concluded [67] that: *weak halogen bonds are basically electrostatic in nature, while strong halogen bonds have some degree of covalent character*. The role of the benzene π-system [68] as electron donor toward halogen (Cl or Br) containing hydrocarbons and

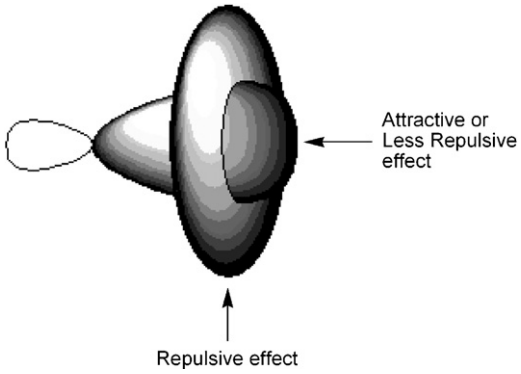

Fig. 1. Schematic representation of the electrostatic potential in covalently bound Cl, Br and I atoms.

fluorocarbons has also been investigated with the same kind of approach. The study concluded that dispersion forces should be the main contribution to the stabilization of the systems as suggested by the large gain of the attraction by electron correlation. Moreover, the charge transferred between the molecules was very small, therefore the charge-transfer contribution should be negligible.

2.2. Electrostatic potential analysis

Brinck et al. [69,70] suggested the use of quantum chemical electrostatic derived potential as a tool to infer the interaction behaviour in the case of XB interactions. According to the analysis halogen atoms linked to less electronegative atoms show electrostatic potential computed at the van der Waals distance with definite anisotropy. In particular, there is a torus of negative potential encircling the halogen atoms. The heavier halogens I, Br, and Cl are further characterized by volumes of positive potential at the side opposite the covalently bound atom (Fig. 1) while this positive crown does not usually appear in fluorine atoms. Repulsive and attractive interactions develop if an electron rich moiety (XB donor site) approaches the halogen on the torus and the crown, respectively.

This model that can explain both the electron donating and accepting ability of C–X with X = Cl, Br, I [71], has been used by Zordan et al. [62] in modelling the interactions where halogen atoms are directly linked to a transition metal, in particular to square planar Pd complexes, and behave as electron donor moieties in the formation of HBs. The same group [35,47] used the approach to rationalize the ability of transition metal bound halogen atoms to behave as XB acceptor groups. According to their studies the halogen atoms show akin distribution of the electrostatic potential as is case of C–X bond even when linked to the Pd atom although in the latter case the negative potential is by far more intense. Furthermore, the modulation of the anisotropy of the interaction along the halogen series is explained using a simple HMO model in which the degree of back-donation is dependent on the strength of the interaction between the p halogen atom orbital and the d ones of the metal influenced by the halogen atom electronegativity (Fig. 2).

This suggests that the degree of polarization of the XB and the degree of anisotropy of the interaction can be modulated by the metal, its coordination sphere, and the suitable halogen atom. This approach, though very useful in rationalizing the HB and XB geometry and intensity of interaction, is the manifestation of a deeper mechanism. In fact the Bader analysis previously discussed shows that a BCP can be observed even in case of low intensity interaction suggesting a reorganization of the electronic density of the whole system whereas the electrostatic potential is evaluated in the non-interacting system.

A deeper mechanism, probably related to the polarization of the electronic cloud responsible for the deshielding of the nuclear charge on the most polarizable group, gives rise to an attraction without significant attractive overlap contribution [46] (i.e., the β contribution at the HMO model or "covalency") when the 4-electron antibonding contribution is overcome and as suggested by the positive value of the $\nabla^2\rho(\mathbf{r})$ obtained in many XB interaction studies both experimental [63] and theoretical as well.

2.3. The valence bond approach

The Valence Bond [72,73] (VB) method in the full formulation and including the polar configuration wave-functions (CW) using non-orthogonal breathing orbitals [74–79] offers an interesting approach to envisage coulombic correlation that is only approximately taken into account at HF-SCF-LCAO level and requires more accurate computations, e.g, MP(n) or CC. Application of this method [80] in the frame of XB has been presented for the F_3^- ion but it, in general, may represent an interesting tool for discussing and interpreting XB [81]. The approach goes further the simple 4-electrons 3-orbitals (4e-3o) HMO method or simple HOMO–LUMO interaction [82] taking into account also different excitation processes, i.e. going beyond the simple single determinant approach. Φ_1 and Φ_5 represent fully covalent, the so called Heitler-London, CW where the electrons that make the bond are singlet-coupled. CW Φ_2, Φ_3, and Φ_4 are ionic. VB shows that even a homopolar bond that links together two identical fragments is never fully covalent, but incorporate some minor ionic terms. Thus, the so-called "Lewis structure" ψ_R that represents the breaking of the "bond" on the

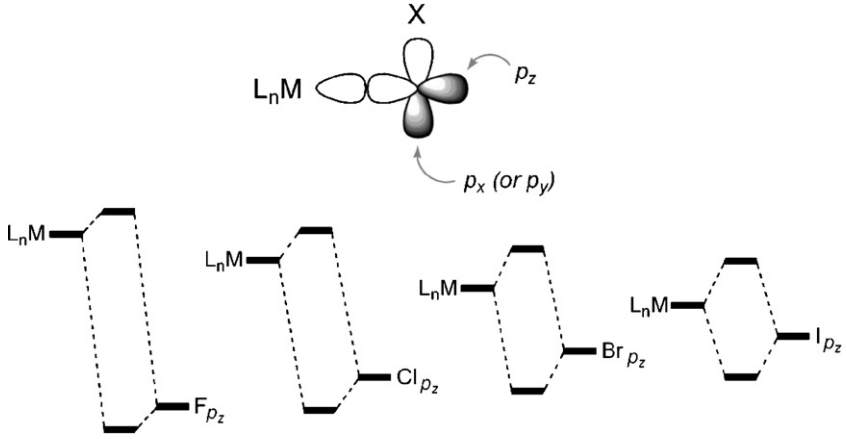

Fig. 2. Schematic representation of the different strength of the interaction between the p_{hal} and the d_{metal} orbitals.

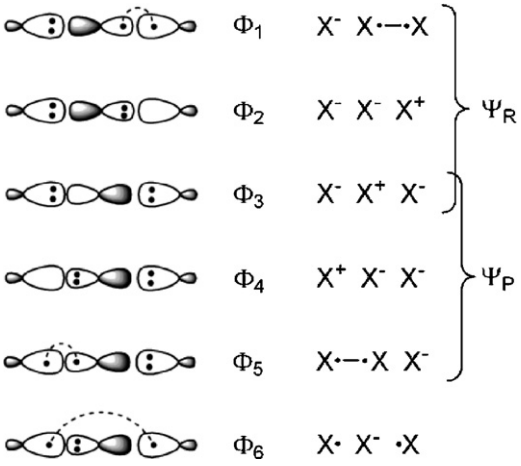

Fig. 3. Schematic representation of the CW involved in the F_3^- ion according to VB approach.

right is a variationally optimized mixture of Φ_1, Φ_2, and Φ_3, while the "bond" on the left is "Lewis structure" ψ_P, which is an analogous combination of Φ_5, Φ_4, and Φ_3 (Fig. 3). The authors showed [80] that in the interaction between the three fluorine atoms in the F_3^- ion the weight of the six CW reported in Fig. 3 are 0.336, 0.006, 0.062, 0.006, 0.336, 0.256, respectively. This result suggests the role of Φ_6, which gives large contribution to the full molecular wave-function because it interacts, by virtue of nonzero overlap, with Φ_1–Φ_5 in the geometry of the adduct, and may consequently stabilize the F_3^- ion. From a qualitative point of view the Valence Bond State Correlation Diagrams [83] have been used to justify the equivalent stabilization of the series of X_3^- (X = Cl, Br, I) ions.

2.4. The case of Cp_2MH_2 (M = Mo, W) in XB

Can hydrogen atoms bound to metals be involved in XB? Although the supposed donor ability of metals in Cp_2MH_2 (M = Mo, W) complexes had been long debated [84], recently DFT investigation [85] at the scalar relativistic level has shown that these complexes exhibit Lewis basic behaviour even though this property is not due to the supposed metal lone pairs but to the hydrogen atoms that show some hydride behaviour.

The same complexes have been used [86] to test, from a computational point of view, their ability to interact with a prototypical iodoperfluorocarbon (CF_3I). From a geometrical point of view the M···I distance is 3.767 and 3.786 Å and the distance M–H are 1.698

Fig. 5. Expected geometries for the approach of a neutral organic XB acceptor (left) and a metal-bound halogen atom (right) to an electrophilic C-bound halogen atom.

and 1.706 Å in case of Mo and W, respectively. The QTAIM analysis points out that the iodine atom interacts in a bifurcated way with the two hydrogen atoms. This view is further supported by the presence of (3, +1) ring critical point, BCP3, (two positive eigenvalues of the electron density Hessian) inside the Mo–H–I–H ring as required by the Poincare–Hopf's relation [87] and from the presence of two BCPs between each hydrogen atom and the iodine one (Fig. 4, left). The *in vacuum* interaction energy is −4.1 (−17.15) and −4.3 (17.99) kcal/mol (kJ/mol) for Mo and W complexes, respectively, taking into account the reorganization contribution (i.e., the total destabilization energy of the two fragments in the complex with respect to free molecule, +1.6 kcal/mol (6.69 kJ/mol) for both Mo and W).

The Ziegler–Rauk [46] energy decomposition analysis points out an orbital contribution (−11.7 (−48.95) and −11.3 (47.28) kcal/mol (kJ/mol) for Mo and W respectively) due to a charge transfer from both HOMO and HOMO-3 orbital (Fig. 4, right). The positive value of the $\nabla^2\rho(\mathbf{r})$ of the BCP's suggests that the interaction is not of the covalent type. Furthermore the donation from both HOMO and HOMO-3 suggests that there is a significant charge reorganization within the organometallic moiety.

2.5. General conclusions on XB from a computational point of view

The computational studies surveyed above suggest that molecular electrostatic potential is s a powerful tool in the choice of the interaction fragment to use as building blocks in XB driven crystal engineering both in case of organic and organometallic or coordination compounds. Also from a computational point of view, halogen bonded fragments show shorter distances between the interacting atoms than the sum of their Van der Waals radii. The geometrical disposition of the (Y)C–X′···$XB_{acceptor}$ complex shows a definite preference for angle in the range 150–180° in close analogy with HB (Fig. 5). Furthermore, when the interaction is of the kind M–X···X′–C(Y) it is possible to define two angles, i.e. M–X···X′–C(Y) and X···X′–C(Y). The former (θ_2) shows values close to 90° and the

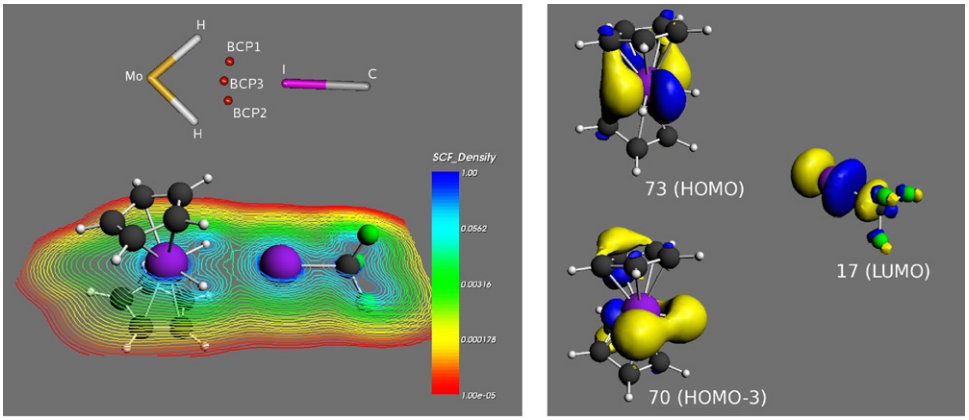

Fig. 4. (left) Bond critical points (BCPs) describing the acid-base interaction and cut plane level curves of the electron density in $Cp_2MoH_2\cdots ICF_3$. The plane is defined by the WH_2 group. A logarithmic scale has been used. (right) Relevant fragment orbitals in the charge donation process of $Cp_2WH_2\cdots ICF_3$. The most important Cp_2WH_2 donor orbitals (73 and 70) and the main ICF_3 acceptor orbital (17) are depicted.

latter (θ_1) close to 180° as it can be expected according to the simple electrostatic model.

Moreover, transition metals in the interacting fragments give rise to a more elaborate contribution than the organic counterparts. Bader analysis is a powerful tool to describe the interaction both when electron density is computed or it is obtained from low temperature X-ray measurements. On the other hand, it appears that further work has to be performed to fully rationalize and understand the different electronic contributions when metallic complexes are involved in the formation of XB.

3. Halopyridinium moieties and congeners

3.1. M–X···X′–C(Py) systems

The ability of metal-bound halogens to behave as strong HB acceptors has been widely described. A great variety of hydrogen-bonded assemblies M–X···H has been obtained [20,88–90] wherein marked differences are observed when X = F rather than Cl, Br and I. The H···X interaction distances typically change in the order F···H ≪ Cl···H ≤ Br···H < I···H for a given HB donor group and HB acceptors X^-, X–M or X′–C, the M–X···H angles depending on both the halogen atom, the metal, and the atom the hydrogen is bound to. Consistently, the trend in HB strength is F···H ≫ Cl···H ≈ Br···H > I···H as confirmed, among others, in the case of an Ir–X···H–N system by using a combination of NMR methods and ab initio calculations [91]. These observations have been interpreted in terms of negative electrostatic potential of M–X moieties associated with a series of compounds. In particular a synthetic strategy for constructing ionic hydrogen bonded materials by combining perhalometallates anions (*e.g.* square planar $[PdCl_4]^{2-}$, tetrahedral $[CdCl_4]^{2-}$, and octahedral $[PdCl_6]^{2-}$ anions) with cations able to serve as HB donors (*e.g.* 4,4′-bipyridine and 1,4-diazabicyclooctane protonated at the nitrogen sites) have been reported [92]. Recently also the robustness of bifurcated HBs of the type M–Cl_2···H–N has been assessed with the synthesis of a series of perchlorometallate salts formed by $[MCl_4]^{2-}$ anions (M = Pd(II), Pt(II)) and bis-cationic systems bearing two protonated nitrogen atoms (*e.g.* 4,4′-H_2-diazastilbene or H_2-*N*-(4-pyridiyl)isonicotinamide [93]).

As an example [94–96] of the numerous cases where analogous series of adducts are obtained when electron donor sites are paired with HB donor or XB donor partners, T. Imakubo and other groups proved that M–X groups can drive the formation of XBs when challenged with a variety of electron poor halocarbons to form M–X···X′–C systems [97,98] where inorganic halogens play a nucleophilic role and organic halogens are the electrophile. Halopyridinium derivatives and other halogenated and positively charged heterocyclic systems have been widely used in order to maximize the difference in electron density between organic and inorganic halogens in M–X···X′–C supramolecular synthons. The electron density of an halogen is obviously dependent on the electron density at the atom it is covalently bound to and the more electron poor the moiety bearing the halogen is, the more pronounced the tendency of the halogen to behave as strong XB donor. A C–X′ moiety will thus work as strong XB donor site when X′ is on a protonated pyridine or on a pyridine coordinated to a metal behaving as a Lewis acid [62] (Scheme 1). The possibility to realize hierarchical self-assembly processes driven in solution and in the solid by interactions of different strength is a peculiar feature of the latter case. In solution well defined mononuclear metal coordinated species (Scheme 1) are formed *via* strong coordination bonds. The structure and geometry of this compound can be designed and suitably tuned in order to achieve the formation, in the solid state, of architectures where the XB, an interaction weaker than standard coordination bonds, assembles the metal coordinated species after pre-established topologies.

In M–X···X′–C systems involving halopyridinium derivatives, the XB has been described to have a strong electrostatic component. Usually the XBs strengths are in the order I > Br > Cl and the X···X′–C and M–X···X′ angles are approximately linear and bent, respectively, in agreement with the relative magnitude and anisotropic nature of the electrostatic potential around the organic and inorganic halogen species. The positive charge on the halopyridinium cation and the negative charge on the halometallate anion play a major role in the strength and directionality of the M–X···X′–C supramolecular synthons [9,99]. Selected examples and data are reported in Table 1.

By reaction of ML_4^{2-} (M = Pd, Pt) with 3-X′-pyridine (X′ = Cl, Br, I) in acidic aqueous solution the corresponding *trans*-$[MCl_2(3\text{-X}'\text{-py})_2]$ have been obtained. Their crystals structures (collected at 150 K) showed the presence of two different networks both characterized by the presence of M–Cl···X′–C interactions [98] (see Table 1): 1D tapes in which each molecule is linked to two neighbours *via* pairs of M–Cl···X′–C interactions (Scheme 2a) and 2D layers in which each molecule is linked to four neighbours *via* individual M–Cl···X′–C interactions (Scheme 2b).

Theoretical and electrostatic potential calculations explained [98] the lack of XBs in *trans*-$[PdCl_2(3\text{-F-py})_2]$, where a repulsive electrostatic contribution to putative M–Cl···F–C interactions would result in a neat repulsive interaction. This behaviour is in agreement with the observation that in general neither short contacts nor orientational preferences are reported for interactions involving C–F groups [100].

The formation of 1D and 2D networks, propagated through "intermolecular" M–X···X′–C XBs, has been reported also on crystallization of *trans*-$[MCl_2(4\text{-X}'\text{-py})_2]$ (M = Pd, Pt; X′ = Cl, Br) and *trans*-$[PdI_2(4\text{-I-py})_2]$ [101]. The X-ray structures (collected at

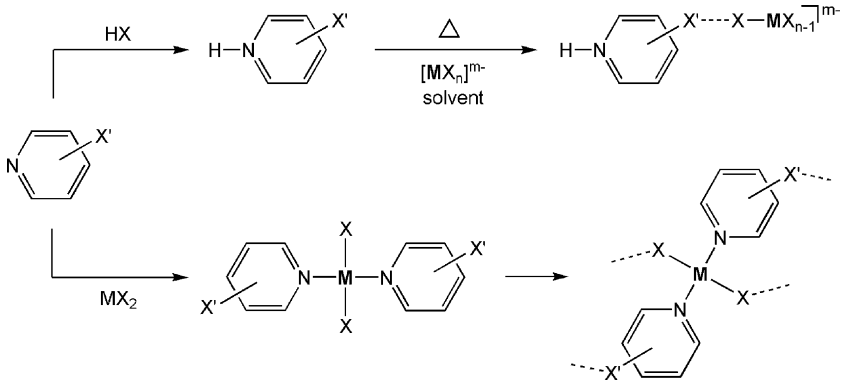

Scheme 1. Strategies for the XB driven self-assembly of halopyridine tectons in the presence of metals.

Table 1
Selected data of halopyridine networks based on XBs[a].

System	Relevant structural data[a]	Network
MCl_4^{2-}/H^+/3-X-py[b]	M = Pt, X = Cl, Br; M = Pd, X = I Pt–Cl···Cl 3.443 Å, C–Cl···Cl 155.9°, Pt–Cl···Cl 92.69° Pt–Cl···Br 3.431 Å, C–Cr···Cl 166.6°, Pt–Cl···Br 126.5° Pd–Cl···I 3.389 Å, C–I···Cl 169.2°, Pd–Cl···Cl 121.98°	1D tapes 2D net
	M = Pt, X = Br; M = Pd, X = Cl, Br Pt–Cl···Br 3.339 Å and 3,3.429 Å, C–Br···Cl 172.0° and 165.7°, Pt–Cl···Br 126.1° and 137.1° Pd–Cl···Cl 3.596 Å, C–Cl···Cl 159.3°, Pd–Cl···Cl 121.1° Pd–Cl···Br 3.534 Å, C–Br···Cl 158.2°, Pd–Cl···Cl 121.69°	
	M = Pt, X = I Pt–Cl···I 3.306 Å, C–I···Cl 170.0°, Pd–Cl···I 131.7°	
MCl_4^{2-}/H^+/4-X-pyH[c]	M = Pt, X = Cl; M = Pd, X = Br Pt–Cl···Cl 3.511 Å, C–Cl···Cl 157.4°, Pt–Cl···Cl 111.6° Pd–Cl···Br 3.516 Å, C–Br···Cl 159.1°, Pd–Cl···Br 112.0°	Tapes and cross-linked tapes 2D net
	M = Pt, X = Br; M = Pd, X = I Pt–Cl···Br 3.325 Å, C–Br···Cl 163.6°, Pt–Cl···Br 85.4° Pd–I···I 3.670 Å, C–I···I 172.1°, Pd–I···I 87.7	
	M = Pd, X = Cl Pd–Cl···H–Cl, 2.599 Å, C–H···Cl 145.4°, Pd–Cl···H 112.5°, C–Cl···Cl–C 3.385 Å, C–Cl···Cl 148.4°	
$CoCl_2\ 6H_2O$/3-X-py/H^+[d]	X = Cl: Co–Cl···Cl 3.441 Å, C–Cl···Cl 169.5°, Co–Cl···Cl 113.4° X = Br: Co–Cl···Br 3.283 Å, C–Br···Cl 170.7°, Co–Cl···Br 92.8° X = I: Co–Cl···I 3.213 Å, C–I···Cl 176.8°, Co–Cl···I 100.7°	1D tapes Ladder chain 2D net (4,4)
$Cu(2\text{-Br-py})Br_2$[e]	Cu–Br···Br 3.460 Å, C–Br···Br 163.36°, Cu–Br···Br 104.68°	Chains‖axis *b*
$Cu(3\text{-Br-py})Br_2$[e]	Cu–Br···Br 3.624 Å, C–Br···Br 161.1°, Cu–Br···Br 118.53°	Chains‖axis *a*
$Cu(2\text{-Br-py})Cl_2$[e]	Cu–Cl···Br 3.358 Å, C–Br···Cl 167.89°, Cu–Cl···Br 103.38°	Chains‖axis *b*
$Cu(3\text{-Br-py})Cl_2$[e]	Cu–Cl···Br 3.622 Å, C–Br···Cl 158.09°, Cu–Cl···Br 120.64°	Chains‖axis *a*
$CuBr_4$/2-Br-py/H^+[f]	Cu–Br···Br 3.449 Å, C–Br···Br 174.2°, Cu–Br···Br 96.8°	1D tapes
$CuBr_4$/3-Br-py/H^+[f]	Cu–Br···Br 3.390 Å, C–Br···Br 179.0°, Cu–Br···Br 119.8°	Ladder chain
$CuBr_4$/4-Br-py/H^+[f]	Cu–Br···Br 3.435 Å, C–Br···Br 174.7°, Cu–Br···Br 114.9°	2D net

[a] Sum of van der Waals radii: Cl–Cl 3.50 Å; Cl–Br 3.60 Å; Cl–I 3.72 Å; Br–Br 3.70 Å, Br–I 3.81 Å, I–I 3.92 Å as reported in ref. [187]; contact distances predicted by the anisotropic model Cl–Cl 3.56 and 3.36 Å; Cl–Br 3.60 Å; Cl–I 3.91and 3.54 Å; Br–Br 3.68 and 3.38 Å, Br–I 3.97and 3.67 Å, I–I 4.26 and 3.89 Å as reported in ref. [188].
[b] See ref. [62].
[c] See ref. [101].
[d] See ref. [97].
[e] X-ray structure collected at 81–85 K. Ref. [99].
[f] X-ray structure collected at 81 K. Ref. [103].

150 K) show the formation of tapes (where each molecule is linked to two neighbours) for *trans*-$[PtCl_2(4\text{-Cl-py})_2]$ and *trans*-$[PdCl_2(4\text{-Br-py})_2]$, whereas 2D layers (where each molecule is linked to four neighbours in a (4,4) grid, giving rise to voids into which the halide ligands from molecules in layers above and below are inserted) are observed in the cases of *trans*-$[PtCl_2(4\text{-Br-py})_2]$ and *trans*-$[PdI_2(4\text{-I-py})_2]$ (Scheme 3). In this last case the size of the hole generated in the 3D net (where iodine ligands are accomodated) are larger than those formed for *trans*-$[PtCl_2(4\text{-Br-py})_2]$, where chloride ligands are employed.

An intriguing application of these materials has been reported showing that the non-porous crystalline solid *trans*-$[CuCl_2(3\text{-Cl-py})_2]$ prepared as a microcrystalline powder, gave reversible HCl uptake under ambient conditions leading to conversion from the initially blue coordination compound to the yellow salt $(3\text{-Cl-pyH})_2[CuCl_4]$ [102].

A series of halogen bonded adducts involving tetrahalocuprate(II) anions and *n*-bromopyridinium cations ($n = 2$, 3, 4) has been described and structures of the adducts clearly show that the $Cu\text{–}X^{-}\cdots Br\text{–}pyH^{+}$ supramolecular synthon is very powerful in determining crystalline structure. The crystal structures consist of isolated planar bromopyridinium cations and distorted tetrahedral CuX_4^{2-} anions forming linear $Cu\text{–}X^{-}\cdots H\text{–}N$ and $Cu\text{–}X^{-}\cdots Br\text{–}C$ contacts, the latter causing significant perturbations on the packing of the ions. When $CuBr_4^{2-}$ and $CuCl_4^{2-}$ are crystallized with n-chloropyridinium cations the X-ray structures for the formed networks show that the $CuCl^{-}\cdots Cl\text{–}pyH^{+}$ supramolecular synthon is a remarkably effective tool in crystal engineering even if weaker than the $Cu\text{–}X^{-}\cdots Br\text{–}pyH^{+}$ supramolecular synthons. The salts $[(CuX_4^{2-})(n\text{-Br-pyH}^{+})_2]_n$ form well defined extended networks of different shape (chains, double chains, 2D networks based on CuX_4^{2-}-$(n\text{-Br-pyH}^{+})_2$-CuX_4^{2-} units) depending on n and halocuprate anion (Scheme 4). The most relevant consequence is the occurrence of π–π stacking and π–Br interactions within the 3D network so that channels and cavities of different dimensions, shape, and polarity are formed within the solid [103].

Zig-zag chains with the cations adopting a stacked arrangement with mutually opposed molecular dipoles occur in the crystal structure of $\{(4\text{-X′-pyH})_2[CoX_4]\}_n$ networks based on $Co\text{–}X\cdots X'\text{–}C$ halogen bonding. The XBs are approximately linear, namely on the elongation of the covalent bond involving the organic halogen atom ($X\cdots X'\text{–}C$ angle in the range 168.6–174.9°). In contrast the $Co\text{–}X\cdots X'$ angles were markedly bent (ranging from 120.3° to 123.7°), the difference between the angles confirming the nucleophilic–electrophilic nature of these interactions and the distinct role of the two halogen atoms [104].

A series of halopyridinium derivatives, including $(4\text{-Cl-pyH})_3[PtCl_6]Cl$, $(4\text{-Cl-pyH})_3[FeCl_4]_2Cl$, $(4\text{-Br-pyH})_3[FeCl_4]_2Cl$, and $(3\text{-I-pyH})_2[AuBr_3X]X$ (X = Cl, Br), has been studied in order to examine the competition between halometallate $[MX_q]^{p-}$ ($q = 4$, 6; $p = 1$, 2) and halide X^- nucleophiles for both XB ($M\text{–}X\cdots X'\text{–}C$) and HB ($M\text{–}X\cdots H\text{–}N$) formation. It was observed that halide anions form stronger HBs than halometallate anions and that HBs are formed in preference to XBs in agreement with the consideration that pyridinium N–H groups are stronger electrophiles than C–X′ groups, thus allowing for stronger interactions. Some intrigu-

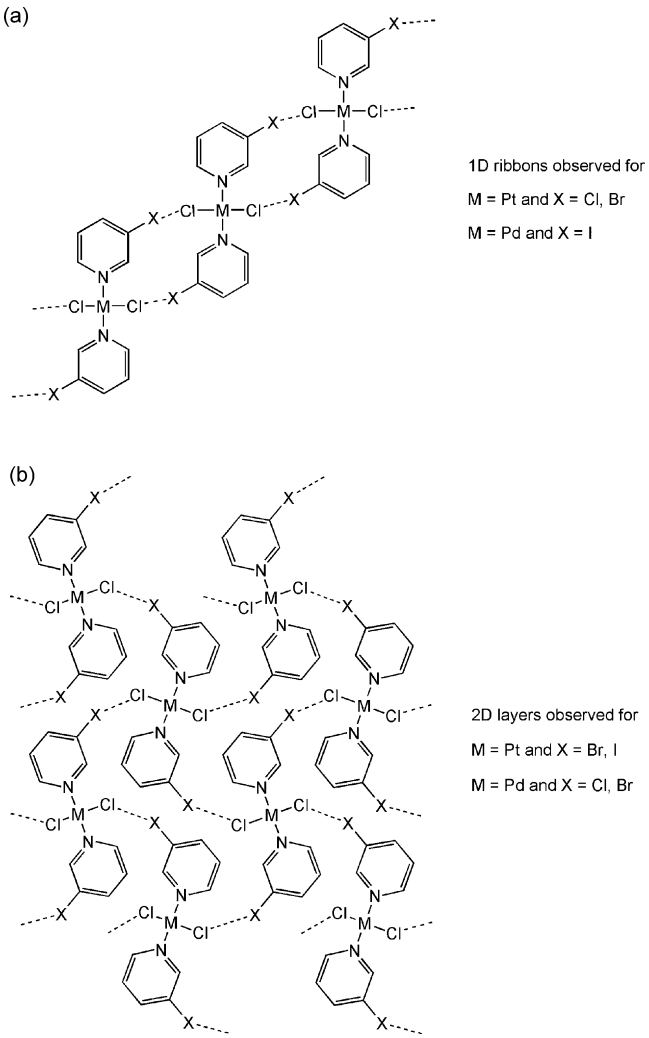

Scheme 2. Schematic representation of the structures of *trans*-[MCl_2(3-X-py)$_2$].

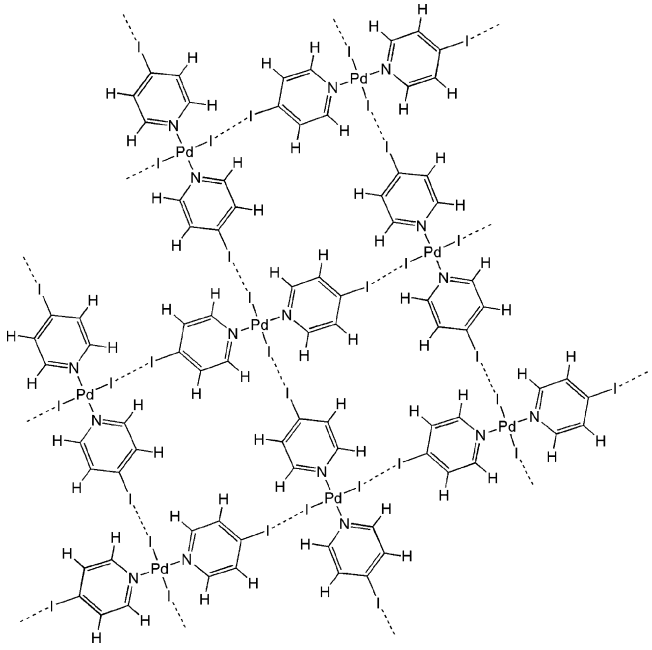

Scheme 3. Schematic representation of the structure of *trans*-[PdI_2(4-I-py)$_2$].

ing observations concern the (3-I-pyH)$_2$[$AuBr_{3.35}Cl_{0.65}$]$Br_{0.30}Cl_{0.70}$ system, the crystal structure of which is characterized by $\{$(3-I-pyH)$_2$[$(Br_{0.30}Cl_{0.70})_n$]$\}^+$ tapes between stacked rows of $[AuBr_{3.35}Cl_{0.65}]^-$ ions with Au–Br···Br–Au contacts of 3.520 Å and Au–Br···Br angles of 159.9° along the chains of ions [105] (Scheme 5).

As a further example of the numerous similarities existing between XB and HB, it is interesting to observe that a series of systems bearing planar pyridinium cations and planar polyhalometallate anions are observed to originate a ribbon motif based on the bifurcated HB synthons $[MCl_2]\cdots$H–N. Remarkably, in (4-Br-pyH)$_2$[$PtCl_6$] [106] and in bis-(3-Br-pyH)[$CuBr_4$] [107] the bifurcated XB synthon $[PtCl]_2\cdots$Br–C is present giving rise to a 3D network, even if, in general, bifurcation of XBs appears to be less common than in HBs, at least in halopyridine systems [108].

AuCl···Br–C XBs (Cl···Br distances 3.441 and 3.384 Å; angles Cl···Br–C angles 173.1° and 169.6°), Au–Cl···H–C HBs, and aurophilic Au···Au interactions have been reported to be present in the 3D network originated by crystallization of bis-(3-Br-pyridine)gold(I) dichloroaurate(I) [109].

The effect of extreme conditions, such as high pressures and low temperatures, has been studied on two isostructural metal–organic salts (4-chloropyridinium)$_2$[CoX_4] (X = Cl, Br) by determining the X-ray structures at nine temperatures from 30 to 300 K and nine pressures from atmospheric pressure to 4.2 GPa. Marked anisotropy in compression was observed upon pressure increase, which reflected the different response of different types of non-covalent interactions associated with different directions within the crystal structures [110].

Halopyridinium species are by far the most studied XB donors in the XB driven formation of metal–organic–supramolecular networks involving protonated organonitrogen derivatives, but other cyclic and acyclic organonitrogen derivatives have also been investigated. For instance, one-dimensional zig-zag chains based on Cl···Cl interactions (Cu–Cl···Cl–C 3.466 Å) are formed on reaction of 1,2-bis(diphenylphosphino)ethane monoxide and 5,7-dimethyl-2-chloronaphtyridine with CuCl in the presence of CH_3CN (Scheme 6) [111].

Other XB organonitrogen donors belong to the stuctural class of the halogen substituted imidazolium [112], imidazolinium [113,114], benzodithiazolium [115], and anilinium [116], derivatives. For instance, Te–Br···BrC and Te–Cl···Cl–C XBs are present in the crystalline structures of 2-haloimidazolium hexahalotellurates(IV) (Scheme 7**)** which are obtained when 2-halo-1,3-diisopropyl-4,4-dimethylimidazolium chloride (X = Cl, Br) is reacted with TeX_4 [117].

An interesting case involving halogenated alkylammonium compounds [118] can be found in halogen bonded hybrid perovskites. The organic–inorganic perovskites are among the most extensively studied families of hybrid crystalline species. They consist of a wide range of inorganic anion layers (each comprised of an extended network of corner-sharing metal halide octahedrons) alternating with a variety of different organic cation layers [119,120]. The structure of the organic and inorganic components, and consequently their energy levels, can be controlled independently and the structural flexibility of these materials entails for their tunable magnetic and electric properties. XB and HB at the organic–inorganic layer interface have been reported to give rise to hybrid perovskites with the general formulae [X–$(CH_2)_2NH_3]_2PbI_4$ (X = Cl, Br, I). The materials have been obtained at room temperature by crystallization from CH_3CN solutions of the halogenated ammonium salts and PbI_2 in 2:1 ratio in the presence of excess HI. The structures are characterized by sheets of corner sharing PbI_6 octahedra alternating with organic cation layers as depicted in Scheme 8 [118].

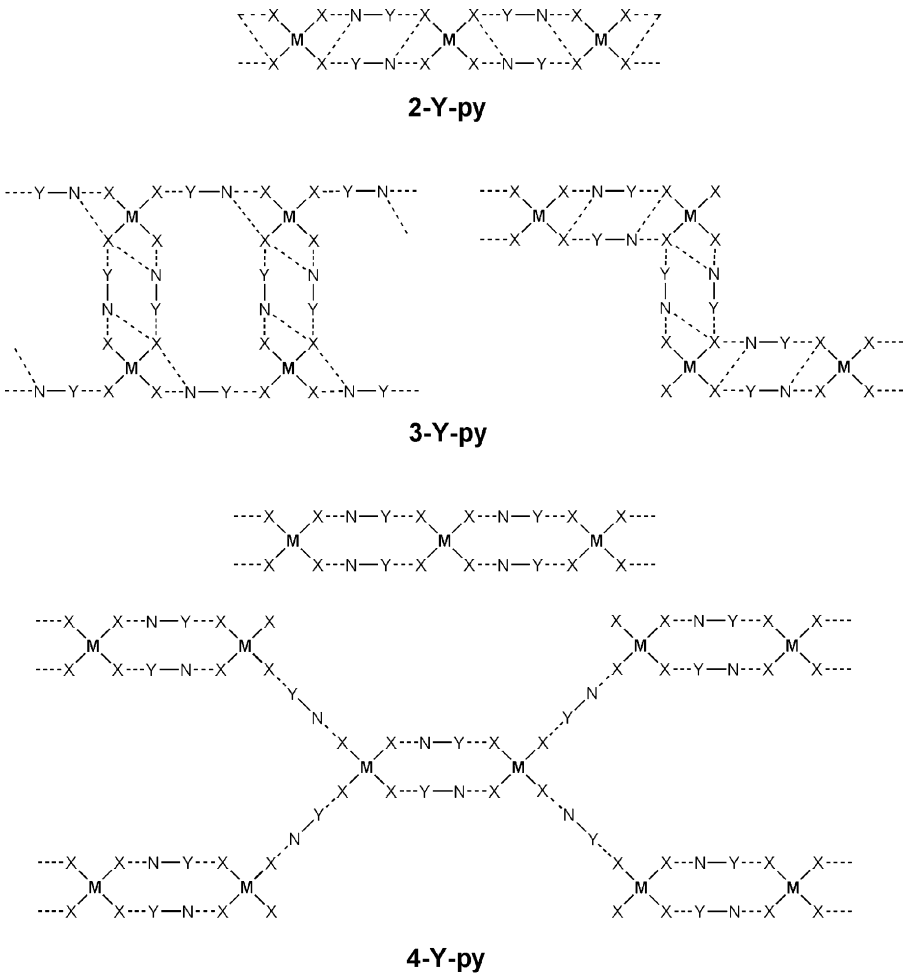

Scheme 4. Schematic representation of the networks based on Cu–X$^{-}\cdots$X′–C and Cu–X$^{-}\cdots$H–N interactions in $[(CuX_4^{2-})(n\text{-}X'\text{-}pyH^{+})_2]_n$ salts (X and X′ = Cl, Br).

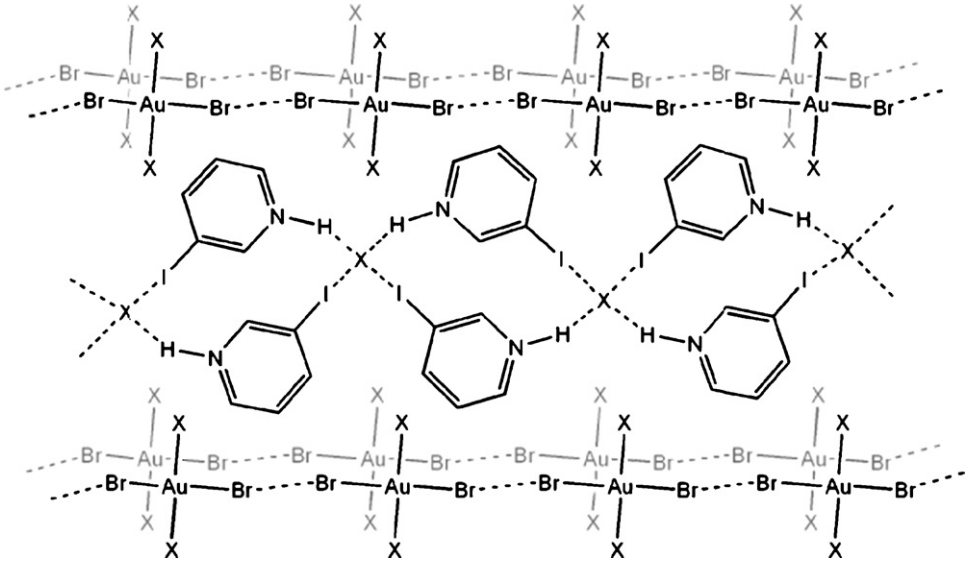

Scheme 5. Schematic representation of $\{(3\text{-}I\text{-}pyH)_2[AuBr_{3.35}Cl_{0.65}]Br_{0.30}Cl_{0.70}\}$.

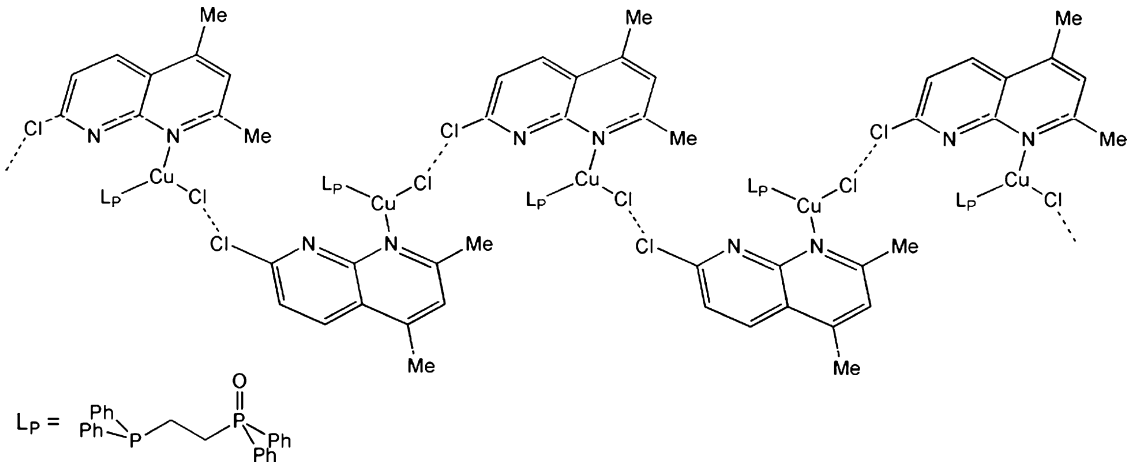

Scheme 6. One dimensional zig-zag chain structure of $[CuL_PLCl]$ (L = 5,7-dimethyl-2-chloronaphtyridine.

A synergistic effect between X···H–N HBs and X···X′–C XBs could explain the structure of perovskite layers which maintain Pb–I–Pb bond angles close to 180°. As a consequence, these red salts display a reduced band gap (2.2 eV) which is assigned to a more dispersed HOMO band compared to other salts based on conventional perovskite layers.

Halogenated carbocations [121] and polyhalomethanes, *e.g.* chloroform [122,123] and dichloromethane [124–126], have also formed halogen bonded adducts with halometallates. TM–X systems (TM = transition metal) show competition between HB and XB [127] when crystallized from chloroform. An example is represented by $[RuCl(CO)\{\eta^2\text{-}C,N\text{-}C_6H_4C(H)=NC_6H_4\text{-}4\text{-}Me\}(PPh_3)_2]$ crystallised by slow evaporation of $CHCl_3$. Both HBs and XBs are present when X = Cl (Scheme 9), when X = Br, I and F only the stronger HBs are observed [128].

Interestingly, tetrabromomethane allowed for the formation of three-dimensional networks characterized by the presence of unusual dodecahedron cells. This topology is well-known in inorganic alloys, but has not been observed before in molecular or hybrid compounds, probably due to the difficulty to construct five-connected nodes from organic derivatives. The self-assembly of tetra *n*-propylammonium dibromocuprate(I) and tetrabromomethane [129] affords an anionic supramolecular network wherein each bromide of the linear $CuBr_2^-$ spaces tetrabromomethane moieties and serves as the five-connected node and each tetrabromomethane represents the four-connected node.

One of the most exciting examples of XB in organometallic systems is obtained when another perhalogenated compound, namely iodopentafluorobenzene, interacts with a Ni–F moiety (Scheme 10).

The formed adduct is one of the few cases where a metal bound fluorine functions as the XB acceptor. As expected, ^{19}F NMR spectra show a downfield shift of the Ni–F signal as a consequence of the interaction with iopentafluorobenzene, similarly to what observed for the titration of the Ni complex with indole, an HB donor. ^{19}F NMR measurements afford also the thermodynamic parame-

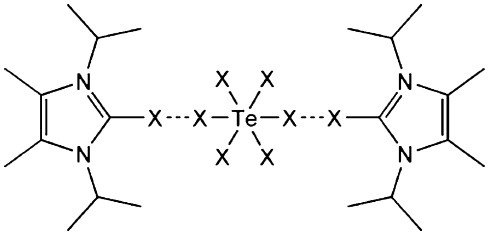

Scheme 7. Schematic structure of the (2-haloimidazolium)$_2$(TeX_6) salt.

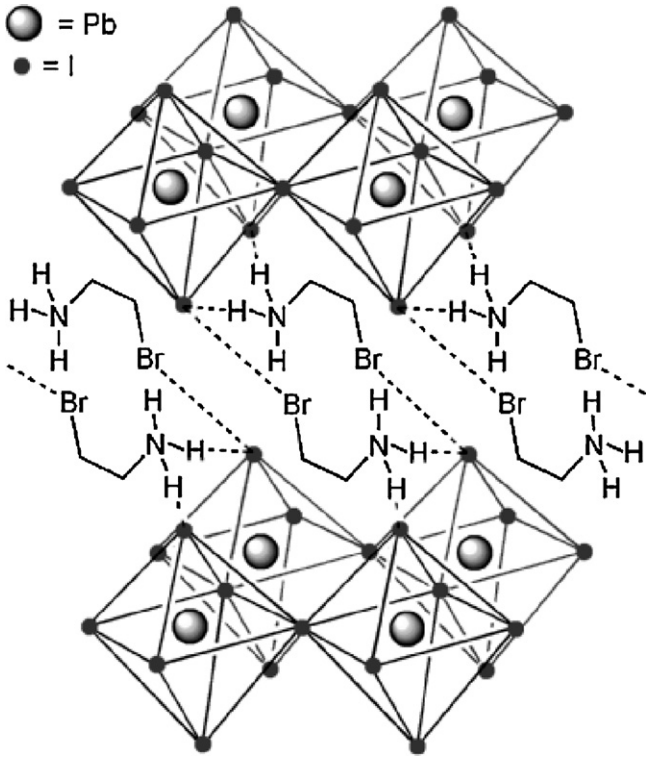

Scheme 8. Schematic representation of the layered hybrid perovskite $[X\text{-}(CH_2)_2\text{-}NH_3]_2PbI_4$.

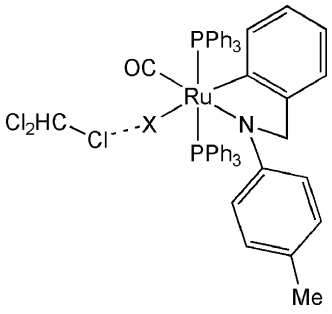

Scheme 9. The XB between $CHCl_3$ and $[RuCl(CO)\{\eta^2\text{-}C,N\text{-}C_6H_4C(H)=NC_6H_4\text{-}4\text{-}Me\}(PPh_3)_2]$.

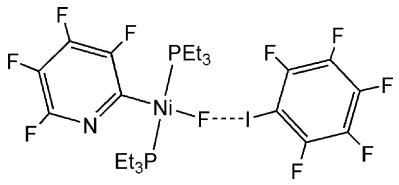

Scheme 10. The XB between *trans*-[NiF(PEt_3)$_2$(2-tetrafluoropyridyl)] and iodopentafluorobenzene.

ters for the interaction. It has been determined that they change significantly with the solvent (ΔH° −16(1) kJ mol^{-1} in toluene-d_8 and −26(1) kJ mol^{-1} in *n*-hexane; ΔS° −42(4) J mol^{-1} K^{-1} in toluene-d_8 and −63(4) J mol^{-1} K^{-1} in *n*-hexane), probably due to specific toluene/iodopentafluorobenzene interactions [130]. This Ni–F···I–C XB can be considered a tool for improving metal-fluoro complexes reactivity. A weakening of the Ni–F bond due to Ni–F···Cl–C interaction might be involved in the substitution of the metal-bound fluorine by a chlorine atom in the reaction of Eq. (1) [131].

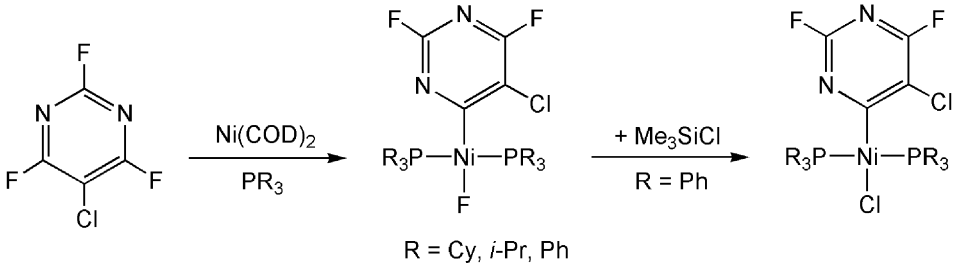

(1)

Chemical and structural differences occur not only on the XB donor side but on the XB acceptor side too. Other polyhalometallates than those described above, have been successfully used for the construction of discrete adducts or infinite networks under XB control (*e.g.* the distorted tertrahedra CrO_3Cl^- [132], $FeCl_4^-$ [17], $InBr_4^-$ [105], $GaCl_4^-$ [133], $CdBr_4^{2-}$ [134], and $NiCl_4^{2-}$ [114], the square bipyramid $NiCl_6^{4-}$ [116], the trigonal bipyramid $SnCl^{5-}$ [122], and other anions having more complex geometry as is the case for $Cu_{10}Br_{22}^{2-}$ [135], $Zn_2Br_6^{2-}$ [126]).

3.2. M–C≡N···X′–C(Py) systems

Percyanometallates and related species have been extensively investigated for their ability to engage as electron-donors in HB formation. Even though less numerous, several structures are available in the Cambridge Structure Database wherein these anions behave as XB acceptors on interactions with organonitrogen cations carrying halogen substituents. This confirms polycyanometallate anions to be exploitable molecular tectons in XB driven crystal engineering [28,136].

When a CH_2Cl_2 solution of [Ru(bipy)(CN)$_4$](PPN)$_2$ (PPN = bis(triphenylphosphoranylidene)ammonium) is mixed with two equivalents of a MeCN solution of (*N*-methyl-3-I-pyridinium)[PF_6], a crystalline adduct is formed whose structure is controlled by quite strong, namely short and linear, Ru–C≡N···I–C XBs (Scheme 11a), the 3D network being originated by aromatic π-stacking [137]. When *N*-methyl-3,5-diiodopyridinum cations are used, also C≡N···I–C XBs involving π electrons of the nitrile residue have been observed (Scheme 11b).

When bromopyridinium salts rather that iodopyridinium are used, the structure changes completely and is dominated by HBs even if C≡N···Br–C XBs are maintained. Cyanometallates can give XBs involving nitrile π electrons also on interaction with brominated partners [138]. As for persistence of Ru–C≡N···X′–C interactions in solutions UV/VIS spectroscopic titrations have been carried out in order to observe the expected blueshift of the Ru[d(π)] → bipy(π*) ^{1}MLCT absorption. A significant blue shift occurred in the two ^{1}MLCT absorptions from 523 to 467 nm and from 364 to 343 nm. The weak luminescence intensity has been interpreted in terms of photoinduced electron transfer in the cation-anion couples present in solution. Ru–C≡N···X′–C XBs represent an intriguing tool to design and modulate luminescent properties of suitable systems for supramolecular photochemistry [137].

As was the case for halometallates, also cyanometallates form XBs with solvent molecules [139,140] and here too the interaction can engage the π electrons of the nitrile residue as is the case, for instance, in Fe–C≡N···Cl–C present in a cyano-tetramesitylporphyrinato-iron(III) chloroform solvate [141]. The robustness of the M-CN···X′–C supramoleculart synthon is proven by the quite short contacts sometimes observed in adducts between polycyanometallate anions and typical chlorinated solvents or chloroaromatics [142].

3.3. MO···X′–C(Py) systems

Cooperative effect of HB, XB, and aryl packing has been used to prepare new inorganic–organic hybrids based on polyoxometallates. When the hydrothermal technique was used, MO···X′–C interactions having different strength have been recognized in supramolecular assemblies formed on interaction of polyoxometallates anions (POM) (*e.g.* [4-(5-(4-Br-Ph)-py-2-yl)pyH]$_4$[$GeW_{12}O_{40}$], [4-(5-(4-Br-Ph)-py-2-yl)pyH]$_4$[β-PMo_8O_{26}], [4-(5-(4-Br-Ph)-py-2-yl)pyH]$_4H_2$[$SiW_{12}O_{40}$] and [4-(5-Cl-py-2-yl)pyH]$_3$[$PMo_{12}O_{40}$]) and halogen substituted bipyridinium cations. The schematic representation of the structure of [4-(5-(4-Br-Ph)-py-2-yl)py]$_4H_2$[$PMo_{12}O_{40}$] is reported in Scheme 12 together with selected data. When POM are of the type [$XM_{12}O_{40}$]$^{n-}$ (X = P, Si, Ge; M = Mo or W) having a α-Keggin-type structure, 1D pillar-like and 2D waved sheets are formed. HBs and XBs give rise to 3D structures of different shape and different packing maps depending n the relative dimensions of the building blocks [143,144]. In the case of Dawson-type POM clusters (such as [α-A-PW_4O_{34}]$^{9-}$ units derived from α-Keggin anion by removal of a set of three corner-shared WO_6 octahedra) the assembly with bipyridyl cations occurs in distorted-wave organic layers. In the presence of electron withdrawing halogen groups on the nitrogen heterocycle, the tendency to form face-to-face π-stacking interactions between nitrogen heterocycles increased and cooperative effect of M–O···H–N and M–O···X′–C interactions directed the ordered assembly templated by POM anions.

4. Tetrathiafulvalenium (TTF) systems and congeners

The strategy to hybridize two components such as organic conducting molecules and transition metal magnetic derivatives has

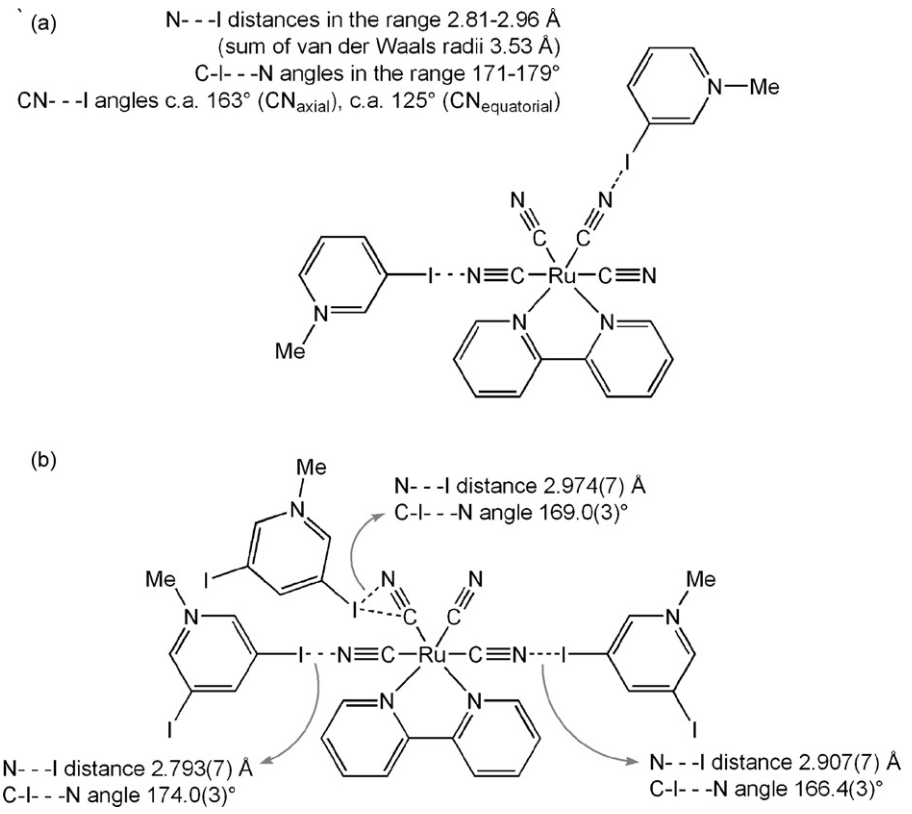

Scheme 11. Schematic representation of the structure of (a) $[N\text{-Me-3-I-py}]_2[Ru(bipy)(CN)_4]$ and (b) $[N\text{-Me-3,5-I,I-py}]_2[Ru(bipy)(CN)_4]$.

been used to develop conducting molecular magnets [32,145–147]. A number of molecular antiferromagnets using tetrathiafulvalene-type derivatives has been developed and their electronic and magnetic properties have been investigated in detail [148].

In the numerous salts of classical tetrathiafulvalene (TTF) and analogues molecules (Chart 2), band dispersion and dimensionality are extremely sensitive to minute modifications of the relative orientations of each independent TTF unit (either in the neutral or radical-cation form). Weak intermolecular interactions, such as HB and XB, are expected to strongly modify such orientations and consequently band structure and associated electronic behaviour. In particular it was observed that the so-called β′slab topology

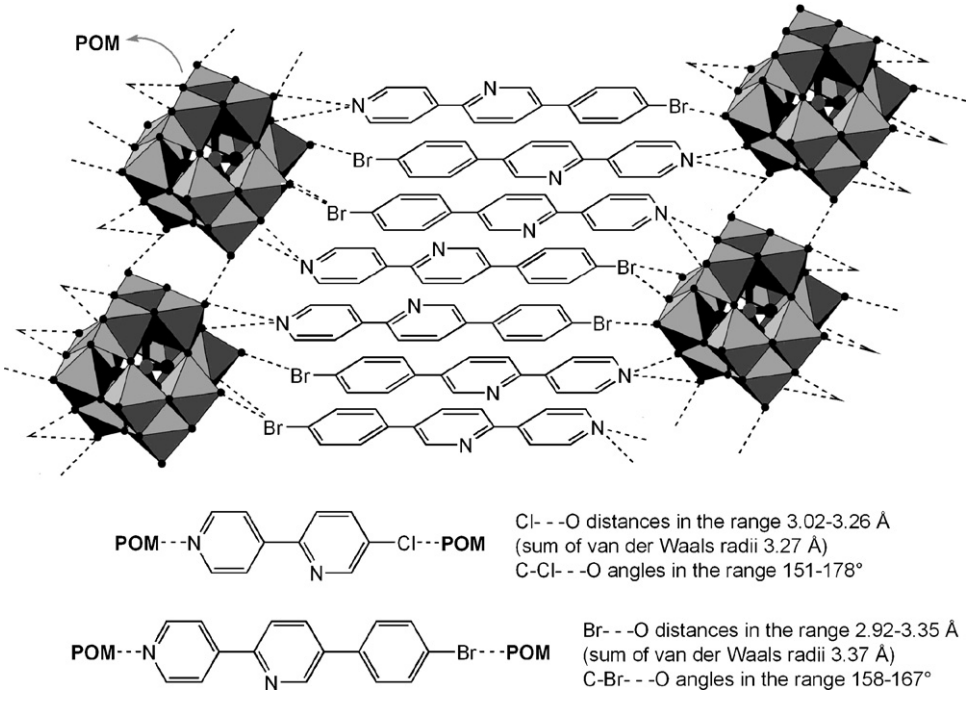

Scheme 12. Schematic representation of the structure of $[4\text{-}(5\text{-}(4\text{-Br-Ph})\text{-py-2-yl})py]_4H_2[PMo_{12}O_{40}]$ and selected data.

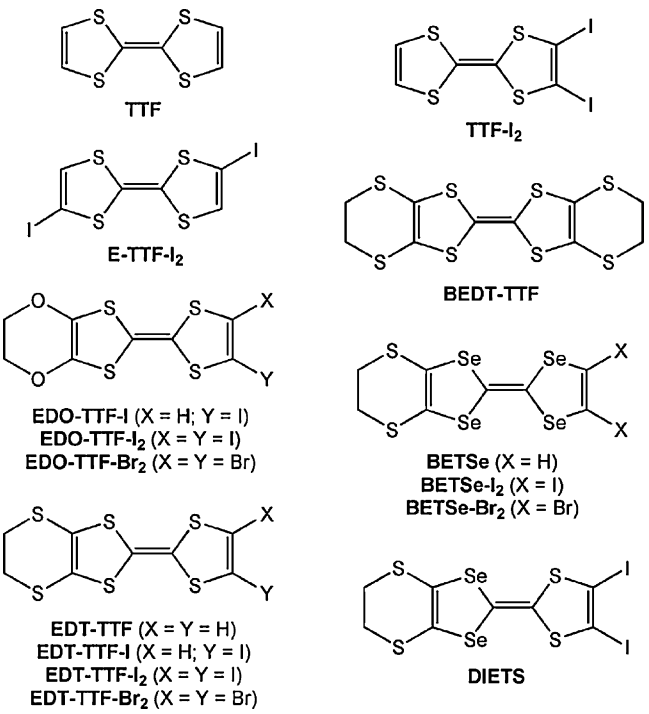

Chart 2.

[149] having localized systems of strongly correlated electrons is characterized by enhanced electrical conductivity and an antiferromagnetic ground state. In the presence of weak interactions able to promote interfacial, organic–organic, and organic–inorganic interactions allowing for the retention of β′ topology, but weakening stack dimerisation, band structure is modified in terms of density of states at the Fermi level, thus improved conductivity and suppression of the antiferromagnetic transition are observed.

Radical cation forms of halogenated derivatives of TTF, and its congeners, can function as particularly strong XB donors so that the interaction has been extensively used to tune the functional properties of the obtained materials. The oxidation of halogenated TTFs (bromo and iodo derivatives in most cases) enhances the partial positive charge on the halogen atom, which then exhibits a remarkably strong tendency to interact with counter ions, acting as Lewis bases, to give short Y···X′–TTF interactions with a wide diversity of anions (Y = halide anions X^-, polyhalides such as I_3^-, polyhalometallates $[MX_n]^{m-}$, polycyanometallates $[M(CN)_n]^{m-}$ and thiocyanate anions). The halogen atom directly linked to the TTF π-system contributes significantly to the HOMO of the molecule and therefore also to the dispersion of the bands deriving from that HOMO, and XB formation thus improves connections of the conducting organic system with the anionic network allowing for a modulation of electronic properties [150].

4.1. M–X···X′–C(TTF) systems

A typical arrangement is depicted in Scheme 13, where the MX_4^{n-} anions control the molecular arrangement achieving a strong π–d interaction with HOMO–HOMO overlap [151]. XBs can determine high symmetrical lattice disposal thus modulating resistivities of the material from metallic, through semiconducting to insulating systems [152].

Ribbons similar to those reported in Scheme 13, or discrete adducts, are obtained also when spherical halide anions are used [153]. The X-ray structure and the physical properties of halogenated tetraselenafulvalenes co-crystals with halometallate counterions have also been reported. The XB donor molecules are uniformly stacked to make quasi 1D columns and the anions are uniaxially elongated from the regular tetrahedron along the twofold axis. In all cases the presence of close intermolecular M–X···X′–TTF contact between the donor columns and anion chains is observed. [122] Some selected data concerning these topics [153–156] are collected in Table 2.

A relevant example is represented by the self-assembly of EDT-TTF-I_2 and covalent polymeric lead iodide motifs to give a layered metallic solid β-$(EDT\text{-}TTF\text{-}I_2)^{+\cdot}[Pb_{5/6}\Upsilon_{1/6}I_2]_3^-$ (Υ = lead vacancy) [157]. The system is characterised by I···I XB distances in the range 3.72–3.75 Å, able to improve interstack interactions, thus increas-

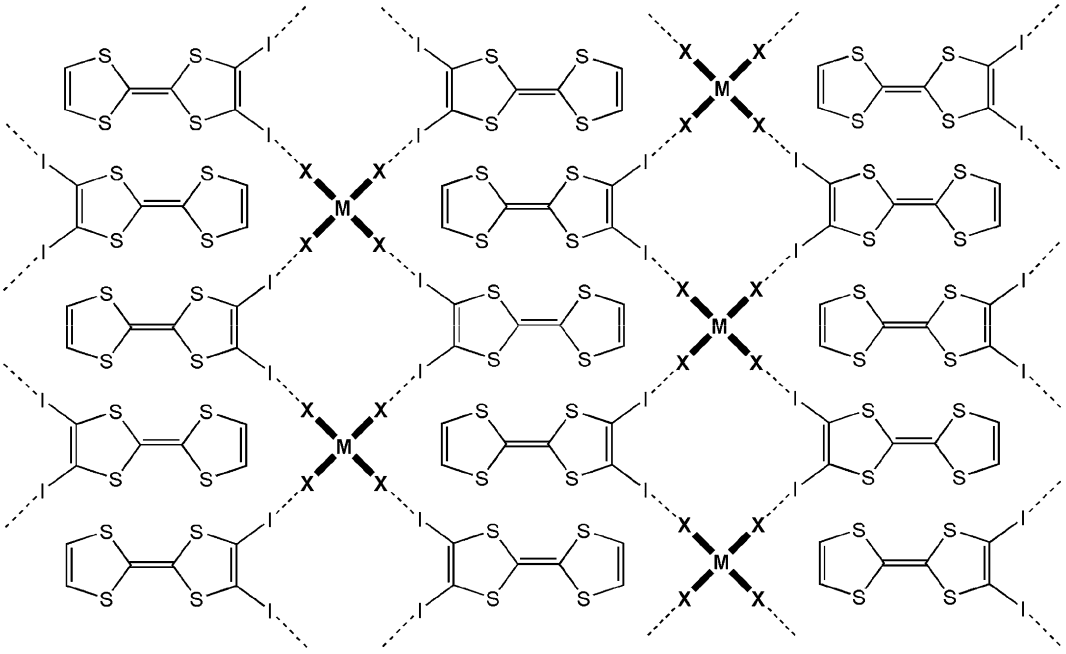

Scheme 13. Typical arrangement of TTF-I_2/MX_4^{n-} systems.

Table 2
Selected data of crystalline networks containing haloTTFs (and analogues) as XB donors.

System	Relevant structural data	T_N[a] (K)	Reference
$(EDT\text{-}TTF\text{-}Br_2)_2FeBr_4$[b]	Br···Br 3.673 and 3.657 Å	11	[166]
$(EDT\text{-}TTF\text{-}Br_2)_2GaBr_4$[b]	Br···Br 3.677 and 3.685 Å		
$(BETSe\text{-}Br_2)_2FeCl_4$[b]	Br···Cl 3.514 Å	2.5	[159]
$(BETSe\text{-}Br_2)_2FeBr_4$[b]	Br···Br 3.649 and 3.645 Å	7.0	
$(BETSe\text{-}Br_2)_2GaCl_4$[b]	Br···Cl 3.532 Å		
$(BETSe\text{-}Br_2)_2GaCr_4$[b]	Br···Br 3.648 and 3.658 Å		
$(EDO\text{-}TTF\text{-}Br_2)_2FeCl_4$	Br···Cl 3.348 Å	4.2	[154,155]
$(EDO\text{-}TTF\text{-}Br_2)_2FeBr_4$	Br···Br 3.432 Å	13.5	
$(EDO\text{-}TTF\text{-}Br_2)_2GaCl_4$	Br···Cl 3.357 Å		
$(EDO\text{-}TTF\text{-}Br_2)_2GaBr_4$	Br···Br 3.507 Å		

[a] Temperature of the antiferromagnetic transition.
[b] X-ray data collected at 293 K.

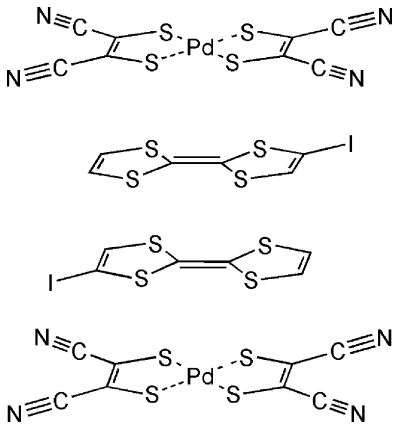

Scheme 15. Stack of ions in the structure of $[I\text{-}TTF^+]_2\{Pd[S_2C_2(CN)_2]\}^{2-}$.

ing interdimer HOMO–HOMO interactions in agreement with the observed resistivity measurements. A conductivity at room temperature of $\sigma_{RT} = 20\ S\ cm^{-1}$ was observed and metallic behaviour was present down to 150 K.

One of the most representative and successful π–d interactions based molecular conducting magnets is λ-$(BETSe)_2MCl_4$ (M = Fe, Ga). In this salt the strong π–d exchange interaction enables a π–d coupled antiferromagnetic state and a field-induced superconductivity [158]. More general and stronger π–d exchange has been proposed to occur when intermolecular halogen···halogen contacts are present and promote exchange interaction between the conducting π-electrons on the donors and the localized d-electrons of the anions. Thus it was reported that $(EDT\text{-}TTF\text{-}Br_2)_2FeBr_4$ undergoes an antiferromagnetic transition of the anion d-spin at 11 K, suggesting the importance of the π–d interaction in the magnetism [159].

4.2. M–C≡N···X′–C(TTF) systems

The first example of a M–C≡N···halogen interaction in radical cation salts of halogenated TTFs was reported by Imakubo and coworkers in the structure of $(EDT\text{-}TTF\text{-}I)_2[Ag(CN)_2]$ where a strong XB was observed (N···I distance of 2.88 Å) arising from the interaction between the lone pair of the nitrogen atom and the σρLUMO on the iodine atom in the arrangement depicted in Scheme 14 [160].

The iodine-based XB appeared to be particularly relevant in the attempt to improve the anisotropic character of organic conducting crystals in order to induce uniaxial strain superconductivity. θ-$(DIETS)_2[Au(CN)_4]$ is a supramolecular superconductor prepared by electrochemical oxidation of a CH_2Cl_2 solution of DIETS in the presence of $[Au(CN)_4](NBu_4)$ as a supporting electrolyte. The X-ray structure of the obtained black crystals show the presence of alternating layers of DIETS cations and square planar tetracyanoaurate anion. Each DIETS molecule functions as bidentate XB donor as each iodine atom on the DIETS is connected to one tetracyanoaurate anion which, on its turn, functions as a tetradentate XB acceptor as two of the four cyano groups function as bifurcated XB acceptors and form two CN···I interactions (N···I distance 3.018 Å, I···N···I angle 97.22°). Interestingly, the superconducting transition temperature Tc of the material was as high as 8.6 K, namely higher than 5 K, the highest known value for unsymmetrical π-donors [161–163].

The electrocrystallization of $EDT\text{-}TTF\text{-}I_2$ and $BETSe\text{-}I_2$ in the presence of $[Fe(CN)_5(NO)]^{2-}$ nitroprusside anions was tried to prepare new materials combining conducting and optical properties [164]. Solids were obtained wherein sheets of adjacent columns of cationic molecules alternated with anions layers. CN···I contacts ranged from 3.08 to 3.25 Å thus indicating the exhistence of fairly strong interactions between the iodine atoms of the XB donor molecules and the cyano group of the cyanometallate counter ion. On the other hand, the interplanar distance longer than the π-cloud thickness suppresses an effective overlap of the π-orbital of the donor molecules along the stacking direction, accounting for a semiconducting behaviour.

Salts of dithiolate derivatives have been co-crystallized with TTF-I. The X-ray crystal structure of $[TTF\text{-}I^+]_2\cdot\{Pd[S_2C_2(CN)_2]\}^{2-}$ adduct shows that the radical cations (D) forms a dimer with an interplanar separation of 3.4 Å. These dimers intermingle with $\{Pd[S_2C_2(CN)_2]\}^{2-}$ anions (A) to form a DDADDA stacked arrangement, connected by nearly linear CN···I–C contact (the CN···I distance is 3.04 Å). The material, over the temperature range from 300 K to 4 K, behaves as a one-dimensional Heisemberg antiferromagnet [165] (Scheme 15).

Segregated stacks of dithiolene cations and cyanometallate anions are connected through XBs also in the salts $(EDO\text{-}TTF\text{-}I_2)_2M(mnt)_2$ (mnt = maleonitriledithiolate; M = Pt, Ni, N···I distance in the range 3.03–3.50 Å for M = Ni and 3.05–3.53 Å for M = Pt) [166]. The resistivity shows metallic behaviour down to 110 K followed by an onset of a metal–insulator transition for both salts, which exhibit also ferromagnetic interaction due to spin polarization effect induced by the orientation-controlled structure.

Salts have been prepared also on cocrystallization of iodine substituted organic π-donors $EDO\text{-}TTF\text{-}I_2$ and $EDT\text{-}TTF\text{-}I_2$, with

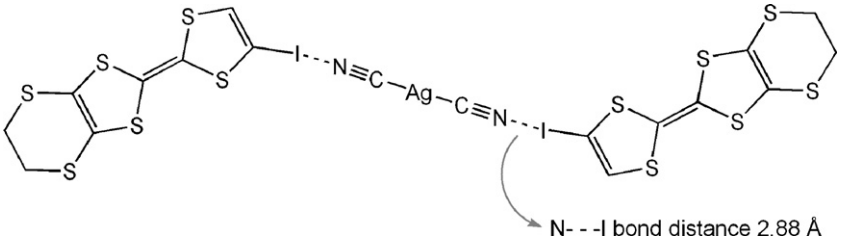

Scheme 14. Schematic representation of the structure of the $(EDT\text{-}TTF\text{-}I)_2[Ag(CN)_2]$ units.

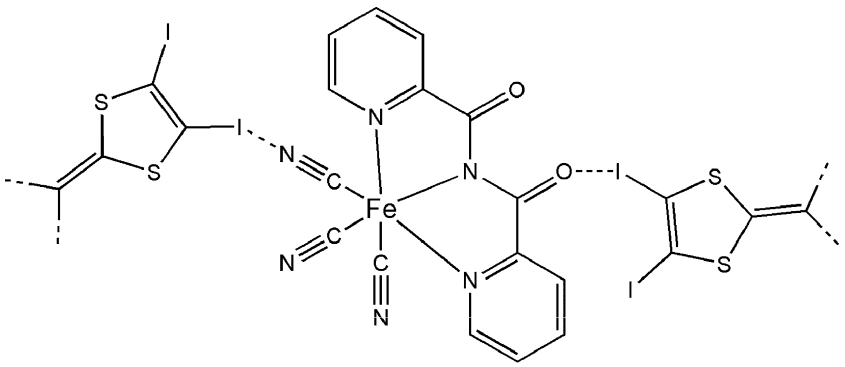

For **EDT-TTF-I_2**
N---I bond distances are 2.989(16), 3.332(20), 2.933(14) Å
O---I bond distance is 2.760(16) Å

For **EDO-TTF-I_2**
N---I bond distances are 3.022(10), 3.279(11), 3.009(10) Å
O---I bond distance is 2.794(8) Å

Scheme 16. Schematic representation of –N···I and –O···I interactions in (EDT-TTF-I_2)[Fe(III)(bpca)$(CN)_3$] and (EDO-TTF-I_2][Fe(III)(bpca)$(CN)_3$].

the paramagnetic [Fe(III)(bpca)$(CN)_3]^-$ anion (bpca = bis(2-pyridylcarbonyl)amide). The crystal structures show the presence of alternate layers of organic (dimerized donor chains) and inorganic units, where interactions between conducting and paramagnetic layers were very short N···I and O···I contacts involving the nitrile and imide moieties, respectively (Scheme 16) [167].

The XB driven self-assembly of the larger cluster anions $[Re_6Se_8(CN)_6]^{4-}$ with EDT-TTF-I and E-TTF-I_2 (an isomer of TTF-I_2, see Chart 2) gave networks supported by Re–CN···I–C XBs. These new materials show very weak antiferromagnetic interactions between spin carriers [168]. The further introduction of the neutral XB donor 1,4-bis-(iodo-ethynyl)benzene into the [EDT-TTF-I^+][$Re_6Se_8(CN)_4]^-$ system in order to affect the structure and tune the physical properties, afforded a new layered material where strong Re–CN···I–C interactions (2.79 Å) govern the self-assembly and develops a one-dimensional polymer out of the octahedral inorganic node [169]. Van der Waals interactions embracing the complementary shapes of the flat, symmetrical neutral aromatic cores and of the cluster anion together with HOMO–HOMO interaction between stacks are also present, allowing for charge carriers delocalization [170].

4.3. M–SCN···X′–C(TTF) systems

EDT-TTF-Br_2 and EDT-TTF-I_2 have been also reported to give salts in the presence of polymeric 1D [Et_4N][$Cd(SCN)_3$] characterized by a two-dimensional segregation of the partially oxidized dithiolene molecules and the polymeric anionic network incorporating embedded solvent molecules. In the case of the EDT-TTF-I_2/[Et_4N][$Cd(SCN)_3$] system two XBs are identified at the organic/inorganic interface and they involve one iodine atom of each of the crystallographycally independent EDT-TTF-I_2 molecules. One iodine is bonded to the nitrogen atom of an acetonitrile molecule embedded in the inorganic layer with N···I distance of 3.023 Å and the other is linked to a thiocyanate sulfur atom (S···I distance of 3.248 Å, the van der Waals S···I distance being 3.72 Å). In this structure (collected at 293 K) each thiocyanate moiety is therefore involved in coordination both through its nitrogen and through

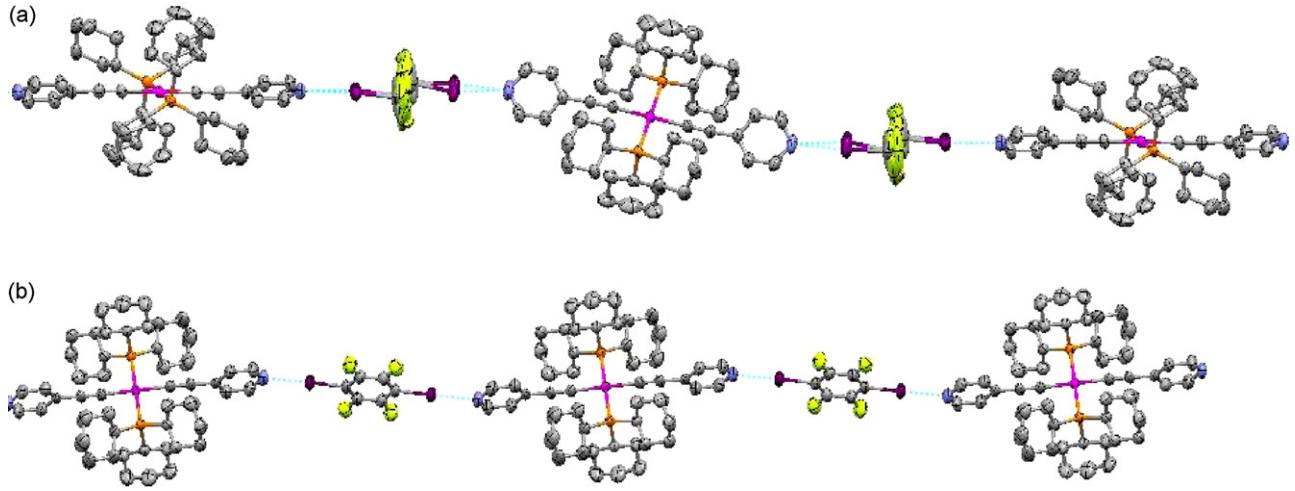

Fig. 6. Ellipsoid view of the linear 1D infinite chains formed in the halogen bonded complexes *trans*-[Pt(P(cy-Hex)$_3$)$_2$(C≡C-4-py)$_2$]/I-CF_2CF_2-I (a) (the tetrafluoroethane moiety is disordered), and *trans*-[Pt(P(cy-Hex)$_3$)$_2$(C≡C-4-py)$_2$]/I-C_6F_4-I. (b) Colours as follows: C, grey; F, green; N, blue; I, magenta; P, orange; Pt, pink. Halogen bonds are dotted sky blue lines. (For interpretation of the references to color in this figure legend, the reader is referred to the web version of the article.)

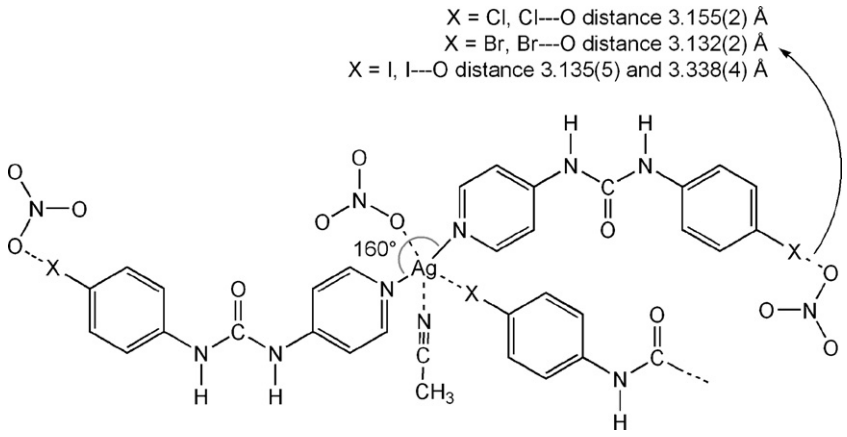

Scheme 17. Schematic representation of contacts in [AgL](MeCN)(NO_3), L = N-4-Cl-phenyl-N′-4-pyridylurea.

its sulfur ends, affording a rigid, two-dimensional porous network, where the empty spaces are filled by two acetonitrile molecules [171].

In the case of the adducts afforded by EDT-TTF-I_2 and DIETS/[M(III)$(isoq)_2(NCS)_4$] (M = Cr, Ga; isoq = isoquinoline), crystal structures show the formation of layered architectures with very short S···I contacts (spanning the range 3.25–3.37 Å). All compounds exhibit semiconductive behaviour with room temperature resistivity ranging from 2×10^3 to $5 \times 10^4\ \Omega$ cm [172].

5. Neutral Metal-organic electron donor systems

Different organometallic derivatives can give rise to coordination networks with quite different topologies related to the different coordination geometries around metal centres. Several cases have been described in previous paragraphs where the metal is sitting at the nodes of the network and its halide or cyanide ligands are involved in transmitting the linear, square planar, or tetrahedral coordination geometry of the metal to the network through XBs. If a metal bears ligands where a spacer separates the metal centre and the XB acceptor, or donor, sites, extra flexibility is added to the geometry of the network in a supramolecular architecture it gives rise to. Despite the virtually unlimited opportunities this type of flexible metal–ligand adducts opens to crystal engineering, few such systems have been reported in the literature.

In this frame we have recently obtained [173] some adducts on co-crystallization of *trans*-[PtL_2(C≡C-4-py)$_2$] (L = tricyclohexylphosphine, PCy_3, triethylphosphine, PEt_3) with 1,2-diiodoperfluoroethane, 1,4-diiodoperfluorobenzene and 4,4′-diiodo-2,2′,3,3′-octafluoro-*trans*-stilbene Eq. (2).

The X-ray structures show that both the organoplatinum derivative and the diodofluorocarbons behave as bidentate and telechelic modules. Quite short, namely strong, N···I contacts drive the formation of one-dimensional unlimited chains (Fig. 6) wherein the XB donor and acceptor modules alternate. The N···I distance can be modulated by changing the phosphine ligand on the metal and the iodofluorocarbon module, these distances being higher for diiodotetrafluoroethane than for bis-perfluoroaryliodides where an extended one-dimensional delocalization occurs (2.83 *vs* 2.70 ↔ 2.80 Å). On increasing the bulkiness of the phosphine ligand (from PEt_3 to PCy_3) the interchain distance nearly doubles. In order to exploit physical properties of these systems based on *trans*-[PtL_2(C≡C-4-py)$_2$] complexes [174] as suitable tools for the preparation of supramolecular metal acetylide polymers, the relationship between structural variations and auxiliary co-ligands around the metal coordination sphere has been investigated. [175,176].

The spacer can separate the metal centre and the XB acceptor site, as is the case of the organoplatinum derivative described above, but examples have also been reported where the spacer separates the metal centre and an XB donor site. For instance, in the solid Cu_2(3-iodobenzoate)$_4$ complex the two oxygen atoms of 3-iodobenzoate anions bridge the two Cu(II) cations and four such bridges form a paddlewheel with the copper ions in the hub. Solvent and cosolvent molecules can enter the metal centres as a fifth ligand. This is the case of dimethylformamide, dioxane, and diazabicycloottane and these ligands are also involved in the formation of intramolecular spacer-O···I-C and spacer-N···I-C XBs which con-

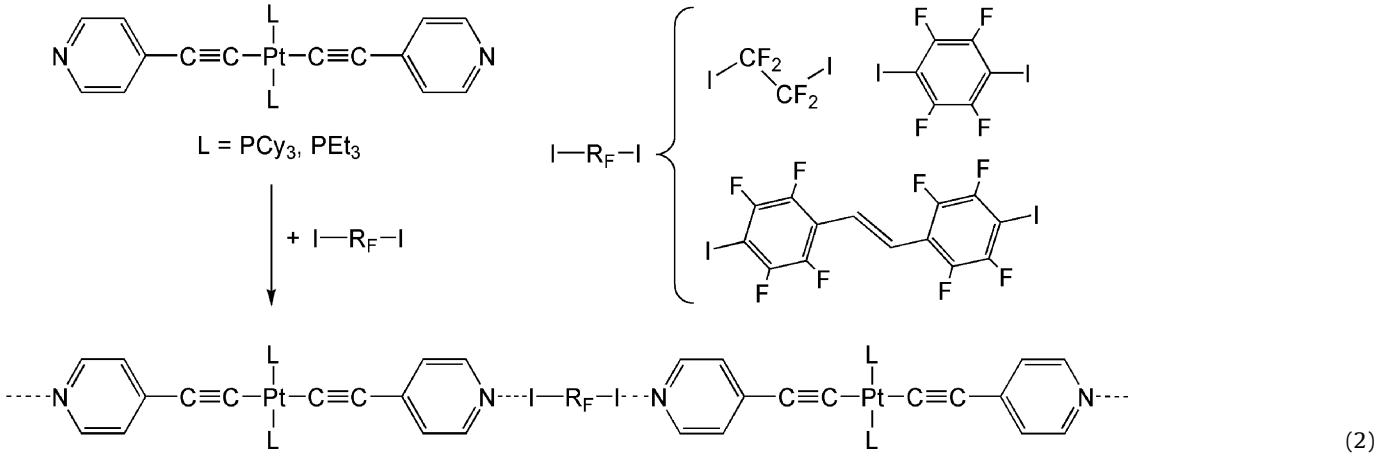

(2)

nect the discrete paddlewhells into one-, two-, or three dimensional networks [177].

The unusual involvement of a nitrate anion as XB acceptor has been observed in low valent coordination compounds. A spacer-X···ONO_2 halogen bonding has been observed in the X-ray structure of [AgL](MeCN)(NO_3) where L = *N*-4-Cl-phenyl-*N*′-4-pyridylurea (Scheme 17) [178].

6. Conclusions

The list of halocarbons known to function as effective XB donor tectons (electron acceptor tectons) is getting longer and longer (*e.g.* bromo- and iodoperfluorocarbons, halopyridinium cations, iodoalkynes, triiodo- and tribromomethane). As far as the nature of XB acceptors is concerned, the most commonly used are neutral molecules substituted with lone-pair possessing heteroatoms. This review, alongside other excellent ones, demonstrates that halogen atoms bound to transition metals or main group metals/metalloids can serve as good XB acceptors, as well. Moreover, metal centers can be conveniently used as platforms for attaching ligands bearing suitable electron donor groups that can be involved in the formation of XB at the outer sphere of metal–ligand complexes.

Our main aim was not to comprehensively review halogen bonded structures involving metal centers. Rather, our aim has been to highlight the possibilities opened in the design and synthesis of new materials by the combined use of XB and coordination bonds. Therefore, some relevant topics have not been purposefully included in this overview, like the chemical behaviour of non-innocent anions such as BF_4^- in terms of XB formation [179]. In our opinion, some other relevant topics appear to be not enough examined until now. This is the case for the understanding of the properties induced by XB introduction in the ligand domain, either from the synthetic or computational point of view. This represents an intriguing challenge for inorganic chemists, together with the understanding of the role played by XB in metalloenzyme chemistry [180].

The profile of XB properties complements the opportunities offered by other interactions more traditionally employed at the outer coordination sphere of metal complexes, like HB. It can be expected that the appreciation of the XB potential in the design of metal–organic complexes will allow for the obtainment of very useful applications in different fields, thanks to the functional properties that can be introduced with the use of a certain metal center, such as redox, magnetic or catalytic properties, and NLO activity. Cooperation of coordination and organometallic chemistry with HB [181,182] and XB [183] represents an intriguing tool for strategic crystal engineering [184] and material design. The specificities in the different fields allow to predict and control the structure of molecular crystals by the directional-bonding, symmetry-interactions and weak-link approaches [185]. The synthesis of functional solid materials by design (even in the presence of polymorphism [186]) becomes possible.

References

[1] P. Metrangolo, F. Meyer, T. Pilati, G. Resnati, G. Terraneo, Angew. Chem. Int. Ed. 47 (2008) 6114.
[2] P. Metrangolo, H. Neukirch, T. Pilati, G. Resnati, Acc. Chem. Res. 47 (2005) 386.
[3] P. Metrangolo, G. Resnati, Chem. Eur. J. 7 (2001) 2511.
[4] W.D. Bruce, P. Metrangolo, F. Meyer, C. Prasang, G. Resnati, G. Terraneo, A.C. Whitwood, New J. Chem. 32 (2008) 477.
[5] P. Metrangolo, G. Resnati, Science 321 (2008) 918.
[6] A. Mele, P. Metrangolo, H. Neukirch, T. Pilati, G. Resnati, J. Am. Chem. Soc. 127 (2005) 14972.
[7] T. Imakubo, M. Kibune, H. Yoshino, T. Shirahata, K. Yoza, J. Mater. Chem. 16 (2006) 4110.
[8] K. Rissanen, CrystEngComm 10 (2008) 1107.
[9] P. Metrangolo, F. Meyer, T. Pilati, G. Resnati, G. Terraneo, Chem. Commun. (2008) 1635.
[10] G. Gattuso, A. Pappalardo, M.F. Parisi, I. Pisagatti, F. Crea, R. Liantonio, P. Metrangolo, W. Navarrini, G. Resnati, T. Pilati, S. Pappalardo, Tetrahedron 63 (2007) 4951.
[11] G. Gattuso, R. Liantonio, P. Metrangolo, F. Meyer, A. Pappalardo, M.F. Parisi, T. Pilati, I. Pisagatti, G. Resnati, Supramolecular Chem. 18 (2006) 235.
[12] T.A. Logothetis, F. Meyer, P. Metrangolo, T. Pilati, G. Resnati, New J. Chem. 28 (2004) 760.
[13] R. Liantonio, P. Metrangolo, T. Pilati, G. Resnati, Cryst. Growth Des. 3 (2003) 355.
[14] P. Metrangolo, T. Pilati, G. Terraneo, S. Biella, G. Resnati, CrystEngComm 11 (2009) 1187.
[15] J.P. Sauvage (Ed.), Transition Metals in Supramolecular Chemistry, J. Wiley & Sons, Baffin Lane, 1999.
[16] U.S. Schubert, M. Heller, Chem. Eur. J. 7 (2001) 5253.
[17] R. Resendes, J.A. Massey, K. Temple, L. Cao, K.N. Power-Billard, M.A. Winnik, I. Manners, Chem. Eur. J. 7 (2001) 2414.
[18] D.G. Kurth, Sci. Technol. Adv. Mater. 9 (2008) 014103.
[19] U.S. Schubert, in: M.K.M.Y. Yagci, O. Nuyken, K. Ito, G. Wnek (Eds.), Tailored Polymers & Applications, VSP Publishers, Utrecht, 2000, p. 63.
[20] D. Braga, L. Brammer, N.R. Champness, CrystEngComm 7 (2005) 1.
[21] L. Brammer, Chem. Soc. Rev. 33 (2004) 476.
[22] D. Braga, Coord. Chem. Rev. 183 (1999) 19.
[23] L. Ma, W. Lin, Angew. Chem. Int. Ed. Engl. 48 (2009) 3637.
[24] S.L. James, Chem. Soc. Rev. 32 (2003) 276.
[25] V.A. Frieze, D.G. Kurth, Coord. Chem. Rev. 252 (2008) 199.
[26] S.J. Dalgarno, N.P. Power, Coord. Chem. Rev. 252 (2008) 825.
[27] S. Kitagawa, R. Kitaura, S. Noro, Angew. Chem. Int. Ed. 43 (2004) 2334.
[28] S.G. Telfer, R. Kuroda, Coord. Chem. Rev. 242 (2003) 33.
[29] C. Piguet, M. Borkovec, J. Hamacek, K. Zeckert, Coord. Chem. Rev. 249 (2005) 705.
[30] M.W. Cooke, D. Chartraud, G.S. Hanan, Coord. Chem. Rev. 252 (2008) 903.
[31] Y. Bodenthin, G. Schwarz, Z. Tomkowicz, M. Lommel, T. Jeue, W. Haase, H. Mohwald, U. Pietsch, D.G. Kurth, Coord. Chem. Rev. (2008), doi:10.1016/j.ccr.2008.10.0199.
[32] E. Coronado, P. Day, Chem. Rev. 104 (2004) 5419.
[33] J.L.C. Rowsell, O.M. Yaghi, Microporous Mesoporous Mater. 73 (2004) 3.
[34] E. Garcia-España, P. Diaz, J.M. Llinares, A. Bianchi, Coord. Chem. Rev. 250 (2006) 2952.
[35] L. Brammer, G.M. Espallargas, S. Libri, CrystEngComm 10 (2008) 1712.
[36] J.C. Mareque Rivas, L. Brammer, Coord. Chem. Rev. 183 (1999) 43.
[37] F. Neese, Coord. Chem. Rev. 253 (2009) 526.
[38] E.K.U. Gross, W. Kohn, Adv. Quantum Chem. 21 (1980) 255.
[39] M.E. Casida, in: D.P. Chong (Ed.), Recent Advances in Density Functional Methods, Pt. 1, vol. 1, World Scientific, Singapore, 1995, p. 155.
[40] A. Szabo, N. Ostlund, Modern Quantum Chemistry, John Wiley and Sons, NY, 1980.
[41] R.J. Bartlett, in: D.R. Yarkony (Ed.), Modern Electronic Structure Theory Part II, Advanced Series in Physical Chemistry, vol. 2, World Scientific, 1987.
[42] A.J. Stone, The Theory of Intermolecular Forces, in: International Series of Monographs on Chemistry, vol. 32, Clarendon Press, Oxford, UK, 2002.
[43] K. Morokuma, K. Kitaura, in: D.G. Politzer, Truhlar (Eds.), Chemical Applications of Atomic and Molecular Electrostatic Potentials, Plenum Press, New York, 1981, p. 215.
[44] T. Ziegler, A. Rauk, Theor. Chim. Acta 46 (1977) 1.
[45] T. Ziegler, A. Rauk, Inorg. Chem. 18 (1979) 1558.
[46] T. Ziegler, in: D.R. Salahub, N. Russo (Eds.), Metal–Ligand Interactions: From Atoms, to Clusters to Surfaces, NATO ASI Series, vol. 378, Kluwer Academic Publishers, Dordrecht, The Netherlands, 1992, p. 367.
[47] E. Scrocco, J. Tomasi, Adv. Quantum Chem. 11 (1978) 116.
[48] A.D. Becke, K.E. Edgecombe, J. Chem. Phys. 92 (1990) 5397.
[49] A. Savin, A.D. Becke, J. Flad, R. Nesper, H. Preuss, H.G. Vonschnering, Angew. Chem. Int. Ed. 30 (1991) 409.
[50] B. Silvi, A. Savin, Nature 371 (1994) 683.
[51] R.F.W. Bader, Atoms in Molecules: A Quantum Theory, Clarendon Press, Oxford, UK, 1990.
[52] A. Karpfen, Struct. Bond 126 (2008) 1 (And references therein).
[53] G. Valerio, G. Raos, S.V. Meille, P. Metrangolo, G. Resnati, J. Phys. Chem. A 104 (2000) 1617.
[54] A.D. Becke, Phys. Rev. A 38 (1988) 3098.
[55] J.P. Perdew, Phys. Rev. B 33 (1986) 8822.
[56] P. Politzer, P. Lane, M.C. Concha, Y. Ma, J.S. Murray, J. Mol. Model 13 (2007) 305.
[57] Hybrid exchange correlation functional are defined as those functional that adds with opportune weight the contribution of the Hartree-Fock exchange contribution to the pure DFT one. See A.D. Becke, J. Chem. Phys. 98 (1993) 5648.
[58] P. Romaniello, F. Lelj, J. Phys. Chem. A 106 (2002) 9114.
[59] E. van Lenthe, A.E. Ehlers, E.J. Baerends, J. Chem. Phys. 110 (1999) 8943.
[60] S.J.A. Van Gisbergen, Molecular response property calculations using time-dependent density functional theory, Ph.D. Thesis, Available online at: http://www.scm.com/Doc/publist.html.
[61] R. van Leeuwen, E.J. Baerends, Phys. Rev. A 49 (1994) 2421.
[62] F. Zordan, L. Brammer, P. Sherwood, J. Am. Chem. Soc. 127 (2005) 5979.

[63] R. Bianchi, A. Forni, T. Pilati, Chem. Eur. J. 9 (2003) 1631.
[64] A. Forni, J. Phys. Chem. A 113 (2009) 3403.
[65] W. Wang, N. Wong, W. Zheng, A. Tian, J. Phys. Chem. A 108 (2004) 1799.
[66] Quotes are in the original paper.
[67] Y.X. Lu, J.W. Zou, Y.H. Wang, Y.J. Jiang, Q.S. Yu, J. Phys. Chem. A 111 (2007) 10781.
[68] Y.X. Lu, J.W. Zou, Y.H. Wang, Y.J. Jiang, Q.S. Yu, Chem. Phys. 334 (2007) 1.
[69] T. Brinck, J.S. Murray, P. Politzer, Int. J. Quantum Chem., Quantum Biol. Symp. 19 (1992) 57.
[70] J.S. Murray, K. Paulsen, P. Politzer, Proc. Indian Acad. Sci. Chem. Sci. 106 (1994) 267.
[71] T. Clark, M. Hennemann, J.S. Murray, P. Politzer, J. Mol. Model. 13 (2007) 291.
[72] N.D. Epiotis, Unified Valence Bond Theory of Electronic Structure, Lecture Notes in Chemistry, vol. 29, Springer Verlag, Berlin, 1982.
[73] G.A. Gallup, Valence Bond Methods, Cambridge University Press, 2002.
[74] P.C. Hiberty, S. Humbel, C.P. Byrman, J.H.J. van Lenthe, Chem. Phys. 101 (1994) 5969.
[75] P.C. Hiberty, S. Humbel, P.J. Archirel, Phys. Chem. 98 (1994) 11697.
[76] P.C. Hiberty, in: E.R. Davidson (Ed.), Modern Electronic Structure Theory and Applications in Organic Chemistry, World Scientific, River Edge, NJ, 1997, p. 289.
[77] P.C. Hiberty, S. Shaik, in: D.L. Cooper (Ed.), Valence Bond Theory, Elsevier, Amsterdam, 2002, p. 187.
[78] P.C. Hiberty, S. Shaik, Theor. Chem. Acc. 108 (2002) 255.
[79] L. Song, Y. Mo, Q. Zhang, W. Wu, J. Comput. Chem. 26 (2005) 514.
[80] B. Braida, P.C. Hiberty, J. Am. Chem. Soc 126 (2004) 14890.
[81] F. Lelj, M. Amati, results to be published.
[82] N. Ramasubbu, R. Parthasarathy, P. Murray-Rust, J. Am. Chem. Soc. 108 (1986) 4308.
[83] S. Shaik, A. Shurki, Angew. Chem. Int. Ed. 38 (1999) 586.
[84] H. Braunschweig, M. Colling, Coord. Chem. Rev. 223 (2001) 1.
[85] M. Amati, F. Lelj, Can. J. Chem. 87 (2009) 1406.
[86] M. Amati, F. Lelj, results to be published.
[87] K. Collard, G.G. Hall, Int. J. Quantum Chem. 12 (1977) 623.
[88] L. Brammer, E.A. Bruton, P. Sherwood, Cryst. Growth Des. 1 (2001) 277.
[89] L. Brammer, E.A. Bruton, P. Sherwood, New J. Chem. 23 (1999) 965.
[90] L. Brammer, Dalton Trans. (2003) 3145.
[91] E. Peris, J.C. Lee, J.L. Rambo, O. Eisenstein, R.H. Crabtree, J. Am. Chem. Soc. 117 (1995) 3485.
[92] L. Brammer, J.K. Swearinger, E.A. Bruton, P. Sherwood, PNAS 99 (2002) 4956.
[93] D.K. Kumar, A. Das, P. Dastidar, Cryst. Growth Des. 6 (2006) 216.
[94] P. Metrangolo, Y. Carcenac, M. Lahtinen, T. Pilati, K. Rissanen, A. Vij, G. Resnati, Science 323 (2009) 1461.
[95] A.C. Legon, Chem. Eur. J. 4 (1998) 1690.
[96] A.C. Legon, Angew. Chem. Int. Ed. 36 (1999) 2686.
[97] L. Brammer, G.M. Espallargas, H. Adams, CrystEngComm 5 (2003) 343.
[98] G.M. Espallargas, F. Zordan, L.A. Marin, H. Adams, K. Shankland, J. van de Streek, L. Brammer, Chem. Eur. J. 15 (2009) 7554.
[99] F.F. Awwadi, D.D. Willett, S.F. Haddad, B. Twamley, Cryst. Growth Des. 6 (2006) 1833.
[100] J.P. Lommerse, A.J. Stone, R. Taylor, F.H. Allen, J. Am. Chem. Soc. 18 (1996) 3108.
[101] F. Zordan, L. Brammer, Cryst. Growth Des. 6 (2006) 1374.
[102] G.M. Espallargas, M. Hippler, A.J. Florence, P. Fernandes, J. van de Streek, M. Brunelli, W.I.F. David, K. Shamkland, L. Brammer, J. Am. Chem. Soc. 192 (2007) 15606.
[103] F.F. Awwadi, D.D. Willett, B. Twamley, Cryst. Growth Des. 7 (2007) 624.
[104] G.M. Espallargas, L. Brammer, P. Sherwood, Angew. Chem. Int. Ed. 45 (2006) 435.
[105] F. Zordan, S.L. Purver, H. Adams, L. Brammer, CrystEngComm 7 (2005) 350.
[106] F. Zordan, G.M. Espallargas, L. Brammer, CrystEngComm 8 (2006) 425.
[107] D.D. Willett, F. Awwadi, R. Butcher, S. Haddad, B. Twamley, Cryst. Growth Des. 3 (2003) 301.
[108] B.K. Saha, A. Nangia, M. Jaskolki, CrystEngComm 7 (2005) 355.
[109] M. Freytag, P.G. Jones, Chem. Commun. (2000) 277.
[110] G.M. Espallargas, L. Brammer, D.R. Allan, C.R. Pulham, N. Robertson, J.E. Warren, J. Am. Chem. Soc. 130 (2008) 9058.
[111] S. Jin, D. Wang, X. Wang, M. Guo, Q. Zhao, J. Inorg. Organomet. Polym. 18 (2008) 300.
[112] G. Valle, R. Ettorre, Acta Cryst., Sect. C: Cryst. Struct. Commun. 50 (1994) 1221.
[113] I. Diaz, V. Fernandez, J.L. Martinez, L. Beyer, A. Pilz, U. Muller, Z. Naturforsch B 53 (1998) 933.
[114] D. Kremzow, G. Seidel, C.W. Lehmann, A. Furstner, Chem. Eur. J. 11 (2005) 1833.
[115] Y.-M. Zhang, L.-Y. Wang, B.-L. Li, J.-H. Yang, Y. Zhang, J. Mol. Struct. 875 (2008) 527.
[116] M. Wei, R.D. Willett, Inorg. Chem. 34 (1995) 3780.
[117] N. Kuhn, A. Abu-Rayyan, K. Eichele, C. Piludu, M. Steimann, Z. Anorg, Allg. Chem. 630 (2004) 495.
[118] S. Sourisseau, N. Louvain, W. Bi, N. Mercier, D. Rondeau, F. Boucher, J.-Y. Buzare, C. Legein, Chem. Mater. 19 (2007) 600.
[119] D.B. Mitzi, J. Chem. Soc. Dalton Trans. (2001) 1.
[120] N. Louvain, N. Mercier, F. Boucher, Inorg. Chem. 48 (2009) 879.
[121] W. Qiu, L. Li, J. Liu, X. Zheng, Y. Fan, C. Sun, Q. Huang, J. Zhang, Eur. J. Solid State Inorg. Chem. 30 (1993) 1039.
[122] A.J. Boyall, K.B. Dillon, J.A.K. Howard, P.K. Monks, A.L. Thompson, Dalton Trans. (2007) 1374.
[123] C. Jones, P.C. Junk, M. Kloth, K.M. Proctor, A. Stasch, Polyhedron 25 (2006) 1592.
[124] S. Schwarz, M.G. Mestres, E. Niquet, C.F.B. da Silva, J. Strahle, Z. Naturforsch B 59 (2004) 167.
[125] F.A. Cotton, E.V. Dikarev, M.A. Petrukhina, Inorg. Chem. 40 (2001) 5716.
[126] D.J. Darensbourg, S.J. Lewis, J.L. Rodgers, J.C. Yarbrough, Inorg. Chem. 42 (2003) 581.
[127] K.R. Flower, R.G. Pritchard, J.E. Warren, Eur. J. Inorg. Chem. (2003) 1929.
[128] K.R. Flower, L.G. Leal, R.G. Pritchard, J. Organomet. Chem. 690 (2005) 3390.
[129] S.V. Rosokha, J. Lu, T.Y. Rosokha, J.K. Kochi, Chem. Commun. (2007) 3383.
[130] S. Libri, A.A. Jasim, R.N. Perutz, L. Brammer, J. Am. Chem. Soc. 130 (2008) 7842.
[131] A. Steffen, M.I. Sladek, T. Raun, B. Neumann, H.G. Stammler, Organometallics 24 (2005) 4057.
[132] P.A. Lorenzo Luis, P. Martin-Zarza, P. Gili, C. Ruiz-Perez, M. Hernandez-Molina, X. Solans Acta, Crystallogr. Sect. C: Cryst. Struct. Commun. 52 (1996) 1441.
[133] T.M. Barclay, A.W. Cordes, J.R. Mingie, R.T. Oakley, K.E. Preuss, CrystEngComm 2 (2000) 89.
[134] R. Al-Far, B.F. Ali, J. Chem. Cryst. 37 (2007) 333.
[135] S. Haddad, F. Awwadi, R.D. Willett, Cryst. Growth Des. 3 (2003) 501.
[136] M. Formiguè, P. Batail, Chem. Rev. 104 (2004) 5379.
[137] S. Derossi, L. Brammer, C.A. Hunter, M.D. Ward, Inorg. Chem. 48 (2009) 1666.
[138] P. Feng, W. Zhe-Ming, G. Song, Inorg. Chem. 46 (2007) 10221.
[139] D.J. Darensbourg, A.L. Phelps, Inorg. Chim. Acta 357 (2004) 1603.
[140] C.-K. Kuo, I.P.-C. Liu, C.-Y. Yeh, C.-H. Chou, T.-B. Tsao, G.-H. Lee, S.-M. Peng, Chem. Eur. J. 13 (2007) 1442.
[141] J. Li, B.C. Noll, C.E. Schulz, W.R. Scheidt, Inorg. Chem. 46 (2007) 2286.
[142] Y. Yamashita, M. Tomura, M.B. Zaman, K. Imaeda, Chem. Commun. (1998) 1657.
[143] Z. Han, Y. Zhao, S. Peng, A. Thian, Q. Liu, J. Ma, E. Wang, N. Hu, Cryst. Eng. Commun. 7 (2005) 380.
[144] Z. Han, Y. Gao, X. Zhai, S. Peng, A. Thian, Y. Zhao, C. Hu, Cryst. Growth Des. 9 (2009) 1225.
[145] R.P. Shibaeva, E.B. Yagubskii, Chem. Rev. 104 (2004) 5347.
[146] H.M. Yamamoto, RIKEN Rev. 46 (2002) 3.
[147] R. Kato, T. Imakubo, H. Yamamoto, R. Maeda, M. Fujiwara, J.I. Yamaura, H. Sawa, Mol. Cryst. Liq. Cryst. 380 (2002) 61.
[148] K. Okabe, J.L. Yamaura, A. Miyaraki, T. Enoki, J. Phys. Soc. Jpn. 74 (2005) 1508.
[149] T. Mori, Bull. Chem. Soc. Jpn. 71 (1998) 2509.
[150] A. Miyazaki, K. Enomoto, K. Okabe, H. Yamazaki, I. Nishijo, T. Enoki, E. Ogura, K. Ugawa, Y. Kuwatani, M. Iyoda, J. Solid State Chem. 168 (2002) 547.
[151] P. Domerq, T. Devic, M. Formiguè, P. Auban-Senzier, E. Canadell, J. Mater. Chem. 11 (2001) 1570.
[152] T. Imakubo, M. Kibune, H. Shirahata, K. Yoza, J. Mater. Chem. 16 (2006) 4110.
[153] T. Imakubo, T. Shirahat, K. Hervè, L. Ouahab, J. Mater. Chem. 16 (2006) 162.
[154] J. Nishijo, A. Miyazaki, T. Enoki, R. Watanabe, Y. Kuwatani, M. Iyoda, Inorg. Chem. 44 (2005) 2493.
[155] A. Miyazaki, H. Yamazaki, M. Aimatsu, T. Enoki, R. Watanabe, E. Ogura, Y. Kuwatani, M. Iyoda, Inorg. Chem. 46 (2007) 3353.
[156] M. Formiguè, Curr. Opin. Solid State Mater. Sci., 2009, doi:10.1016/j.cossms.2009.05.001.
[157] T. Devic, E. Canadell, P. Auban-Senzier, P. Batail, J. Mater. Chem. 14 (2004) 135.
[158] H. Fujiwara, E. Fujiwara, Y. Nakazawa, B.Z. Narymbetov, K. Kato, H. Kobayashi, A. Kobayashi, M. Tokumoto, P. Casson, J. Am. Chem. Soc. 123 (2001) 306.
[159] T. Shirahata, M. Kibune, M. Maesato, T. Kawashima, G. Saito, T. Imakubo, J. Mater. Chem. 16 (2006) 3381.
[160] I. Imakubo, H. Sawa, R. Kato, Synth. Met. 73 (1995) 117.
[161] T. Imakubo, N. Najima, M. Tamura, R. Kato, Y. Nishio, K. Kajita, J. Mater. Chem. 12 (2002) 159.
[162] T. Imakubo, A. Miyake, H. Sawa, R. Kato, Synth. Met. 120 (2001) 927.
[163] T. Imakubo, T. Shirahata, M. Kibune, H. Yoshino, Eur. J. Inorg. Chem. (2007) 4727.
[164] K. Ueda, T. Sugimoto, C. Faulmann, P. Cassoux, Eur. J. Ing. Chem. (2003) 2333.
[165] A. Batsanov, A.J. Moore, N. Robertson, A. Green, M.R. Bryce, J.A.K. Howard, A.E. Underhill, J. Mater. Chem. 7 (1997) 387.
[166] J. Nishijo, E. Ogura, J. Yamaura, A. Miyazaki, T. Enoki, T. Takano, Y. Kuwatani, M. Iyoda, Solid State Commun. 116 (2000) 661.
[167] L. Ouahab, F. Setifi, S. Golhen, I. Imakubo, R. Lescouezec, F. Floret, M. Julve, R. Swetlik, C. R. Chim. 8 (2005) 1286.
[168] A. Ranganathan, A. El-Ghayoury, C. Meziere, E. Hartè, R. Clerac, P. Batail, Chem. Commun. (2006) 2878.
[169] H.M. Yamamoto, J.I. Yamaura, R. Kato, J. Mater. Chem. 8 (1998) 15.
[170] A.L. Barriers, A. El-Ghayoury, L.V. Zorina, E. Canadell, P. Auban-Senzier, P. Batail, Chem. Commun. (2008) 2194.
[171] M. Formigue, P. Auban-Senzier, Inorg. Chem. 47 (2008) 9979.
[172] K. Hervè, O. Cador, S. Golhen, K. Costuas, J.F. Halet, T. Shirahata, T. Muto, T. Imakubo, A. Miyazaki, L. Ouahab, Chem. Mater. 18 (2006) 790.
[173] G. Terraneo, P. Sgarbossa, G. Resnati, R. Bertani, T. Pilati, results to be published.
[174] Y.K. Kryschenko, S. Russel Seidel, A.M. Arif, P.J. Stang, J. Am. Chem. Soc. 125 (2003) 5193.
[175] R. Ziessel, M. Hissler, A. El-chayoury, A. Harriman, Coord. Chem. Rev. 178–180 (1998) 1251.
[176] W.Y. Wong, C.L. Ho, Coord. Chem. Rev. 250 (2006) 2627.

[177] P. Smart, G.M. Espallargas, L. Brammer, CrystEngComm 10 (2008) 1335.
[178] S.K. Chandran, R. Thakuria, A. Nangia, CrystEngComm 10 (2008) 1891.
[179] G. Bellachioma, G. Ciancaleoni, C. Zuccaccia, D. Zuccaccia, A. Macchioni, Coord. Chem. Rev. 252 (2008) 2224.
[180] J.M. Rubin-Preminger, U. Englert, Inorg. Chim. Acta 362 (2009) 1135.
[181] D. Natale, J.C. Mareque-rivas, Chem. Commun. (2008) 425.
[182] R.K. Feller, A.K. Chetham, CrystEngComm 11 (2009) 980.
[183] E. Corradi, S.V. Meille, M.T. Messina, P. Metrangolo, G. Resnati, Angew. Chem. Int. Ed. 39 (2000) 1782.
[184] G.R. Desiraju, Angew. Chem. Int. Ed. 46 (2007) 8342.
[185] B.J. Holliday, C.A. Mirkin, Angew. Chem. Int. Ed. 40 (2001) 2022.
[186] D. Cincic, T. Friscic, W. Jones, Chem. Mater. 20 (2008) 6623.
[187] A.J. Bondi, J. Phys. Chem. 68 (1964) 441.
[188] S.C. Nyburg, C.H. Faerman, Acta Crystallogr. B 41 (1985) 274.